A Review of Surface-Based Microwave and Millimeter-Wave Radiometric Remote Sensing of the Troposphere

E.R. Westwater
S. Crewell
C. Mätzler

Abstract

Surface-based radiometric sensing of tropospheric parameters has a long history of providing useful measurements of temperature, water vapor, and cloud liquid. In this review, a general overview of physical fundamentals, measurement techniques, and retrieval methodology is given. Several contemporary instruments are then discussed and representative results are presented. Recent and promising developments include multi-frequency radiometers, scanning observations of clouds, and combined active-passive remote sensing. The primary applications of these new technologies are weather forecasting and climate, communications, geodesy and long-baseline interferometry, satellite data validation, air-sea interaction, and fundamental molecular physics.

1. Introduction

Surface-based radiometric measurements of atmospheric thermal emission have proven useful in a variety of meteorological applications, including meteorological observations and forecasting, communications, geodesy and long-baseline interferometry, satellite validation, climate, air-sea interaction, and fundamental molecular physics. One reason for the utility of these measurements is that with careful design, radiometers can be operated in a long-term unattended mode in nearly all weather conditions [1, 2, 3]. The measurements also enable the continued development of absorption and radiative transfer models in both clear [4, 5] and cloudy [6] atmospheres. This development has been greatly aided by long-term, carefully calibrated radiometer measurements, supplemented by frequent radiosonde releases using active sensors for cloud identification [7, 8]. Last but not least is the development of retrieval and data assimilation algorithms [9, 10], with which radiometer data can be combined with external data sources, such as forecasts or soundings from active sensors. In this overview of surface-based radiometers, we confine our attention to radiometric soundings of water vapor, temperature, and clouds in the troposphere.

2. Microwave Absorption and Emission

The principal sources of atmospheric emission and absorption are water vapor, oxygen, and cloud liquid. In the frequency region from 20 GHz to 200 GHz, water-vapor absorption arises from the weak absorption line at 22.235 GHz and the much stronger line at 183.31 GHz. In addition, the so-called continuum absorption of water vapor arises from the far wing contributions from higher-frequency resonances that extend into the infrared region. In the frequency band from 50 GHz to 70 GHz and the region about 118 GHz, oxygen absorbs due to a series of magnetic dipole transitions centered around 60 GHz and the isolated line at 118.75 GHz. Because of pressure broadening, the oxygen absorption extends outside of the immediate frequency region of the resonant lines. There are also resonances by ozone that are important for stratospheric sounding [11]. In addition to gaseous absorption, scattering,

Ed R. Westwater is with the Cooperative Institute for Research in Environmental Sciences, University of Colorado/NOAA Environmental Technology Laboratory, 325 Broadway MS R/E/ET1, Boulder, CO, 80305 USA; Tel: +1 (303) 497-6527; Fax: +1 (303) 497-3577; E-mail: Ed.R.Westwater@noaa.gov; http://www.etl.noaa.gov/~ewestwater
Susanne Crewell is with the Meteorologisches InstitutUniversitaet Muenchen, Theresienstr. 37 80333 Muenchen, Germany;
Tel: +49 (0) 89/2180-4210; Fax: +49 (0) 89/2805508; E-mail: crewell@meteo.physik.uni-muenchen.de; http://www.meteo.physik.uni-muenchen.de/.
Christian Mätzler is with the Institute of Applied Physics, University of Bern, Sidlerstr. 5, CH-3012 Bern, Switzerland; Tel: +41 31 631 45 89; Fax: +41 31 631 37 65; E-mail: matzler@iap.unibe.ch; http://www.iapmw.unibe.ch.

Editors Note: This is one of the invited *Reviews of Radio Science*, from Commission F.

absorption, and emission also originate from hydrometeors in the atmosphere. Our focus in this article is on non-precipitating clouds, for which emission and absorption are of primary importance.

2.1 Gaseous Absorption Models

Detailed calculations of absorption by water vapor and oxygen were first published by J. H. Van Vleck. The quantum mechanical basis of these calculations, including the Van Vleck-Weisskopf line shape, together with laboratory measurements, have led to increasingly accurate calculations of gaseous absorption. Both these historical and recent developments are discussed in [12]. Currently, there are three absorption models that are widely used in the propagation and remote-sensing communities. Starting with laboratory measurements that were made in the late 1960s and continuing for several years, H. Liebe developed and distributed the computer code of his Microwave Propagation Model (MPM). One version of the model [13] is still extensively used, and many subsequent models are compared with this one. Liebe later made changes to both water-vapor and oxygen models, especially to parameters describing the 22.235 GHz H_2O line and the so-called water-vapor continuum [14]. More recently, Rosenkranz [5a, 5b] developed an improved absorption model that also is extensively used in the microwave propagation community. However, there are many issues in the determination of parameters that enter into water-vapor-absorption modeling, and a clear discussion of several of these issues is given in [5]. Relevant to the discussion is the choice of parameters to calculate the pressure-broadened line width, which, in the case of water vapor, arises from the collisions of H_2O with other H_2O molecules (self broadening), or from collisions of H_2O molecules with those of dry air (foreign broadening). In fact, Rosenkranz [5a, 5b] based his model on using Liebe and Layton's [13] values for the foreign-broadened component, and those from Liebe et al. [14] for the self-broadened component. Another model that is used extensively in the US climate research community is the Line by Line Radiative Transfer Model (LBLRTM), by S. Clough and his colleagues[7]. One feature of the Clough model is that it has been compared extensively with simultaneous radiation and radiosonde observations near 20 GHz and 30 GHz.

2.2 Cloud Absorption Models

For spherical particles, the classical method of calculating scattering and absorption coefficients is through the Lorenz-Mie Equations [15, 16, 17]; for sufficiently small particles, the Rayleigh approximation can be used. The particle contribution is calculated for a given wavelength and single particle; the total coefficients are then obtained by integration over the size distribution of particles. An important physical property for the calculations is the complex dielectric constant of the particle. This dielectric constant of liquid water is described by the dielectric relaxation spectra of Debye [18]. The strong temperature dependence of the relaxation frequency is linked to the temperature-dependent viscosity of liquid water; therefore, the cloud-absorption coefficient also shows significant temperature sensitivity. The dielectric constant can be well measured in the laboratory above 0°C, and a variety of measurements have been made from 5 GHz to 500 GHz [6]. However, for super-cooled water – below 0°C – the situation is less certain, and, for example, models of [6, 19, 20] differ by 20% to 30% in this region [21]. This is relevant for cloud remote sensing, because measurements of super-cooled liquid are important for detection of aircraft icing [22]. When calculating absorption for non-precipitating clouds, we assume Rayleigh absorption, for which the liquid absorption depends only on the total liquid amount and does not depend on the drop-size distribution, and scattering is negligible. The Rayleigh approximation is valid when the scattering parameter $\beta = \left|n\left(2\pi r/\lambda\right)\right| \ll 1$ [16]. Here, r is the particle radius, λ is the free-space wavelength, and n is the complex refractive index. For rain and other situations for which the β is greater than roughly 0.1, the full Mie equations, combined with a modeled (or measured) size distribution, must be used.

Due to the non-spherical shape of ice hydrometeors, the situation is more complicated when scattering plays a role. Although this situation is beyond the scope of this article, at millimeter wavelengths the particle size of cirrus clouds can be of the order of 100 to 200 microns, and scattering may be important near transmission windows. On the other hand, the dielectric properties of ice [23, 24] are very different from those of liquid water. The dielectric losses of ice have a minimum near 1 GHz, and ice is an almost perfectly loss-free medium over a large frequency range. Therefore, microwave emission of pure ice particles can be neglected in most cloud situations. Special situations occur when ice particles start to melt. A very thin skin of liquid water can be sufficient to cause significant absorption, and thus emission. Usually, these conditions apply to precipitating clouds, or in the so-called radar "bright band."

2.3 Calculations of Absorption Spectra

For standard conditions at sea level, we calculated the water vapor (H_2O), oxygen (O_2), and total clear ($H_2O + O_2$) contributions to the absorption coefficient. In addition, we calculated the liquid absorption coefficient for $\rho_L = 0.1\ \mathrm{gm}^{-3}$ at $T = 293$ K and 273 K. From the results shown in Figure 1, we note the strong oxygen absorption regions near 60 GHz and 118 GHz due to oxygen, and the large absorption near 183 GHz. For a given location and altitude, the oxygen absorption is relatively constant, with variations of 10% to 20%, while both the 22.235 GHz and the 183.31 GHz absorptions can vary by a factor of 10 to 20. Note also the strong temperature dependence of cloud absorption, and the reversal of this dependence at around 150 GHz.

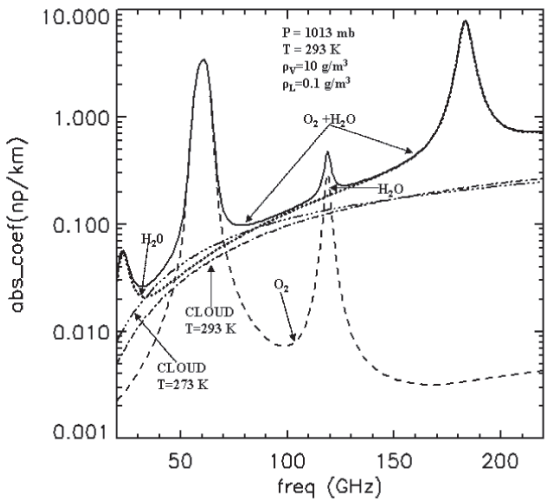

Figure 1. Microwave absorption spectra from 20 GHz to 220 GHz. The absorption models used were Liebe 89 [4] for clear absorption, and Liebe et al. 1991 [6] for cloud liquid. In this figure, P is pressure, T is temperature, ρ_V is absolute humidity, and ρ_L is cloud liquid density.

2.4 Microwave Thermal Emission

Neglecting scattering, we relate our primary observable, brightness temperature, T_b, to the atmospheric state by the radiative transfer equation (RTE) [25]:

$$B_\nu(T_b) = B_\nu(T_c)\exp(-\tau)$$

$$+\int_0^\infty B_\nu\left[T(s)\right]\alpha(s)\exp\left[-\int_0^s \alpha(s')\,ds'\right]ds\,, \quad \text{(1a)}$$

where s is the path length in km, $T(s)$ is the temperature (K) at the point s, and T_c is the cosmic background brightness temperature of 2.75 K. τ = opacity = total optical depth along the path s:

$$\tau = \int_0^\infty \alpha(s)\,ds\,, \quad \text{(1b)}$$

where $a(s)$ is the absorption coefficient (nepers/km) at the point s, and $B_\nu(T)$ is the Planck function at frequency ν and temperature T:

$$B_\nu(T) = \frac{2h\nu^3}{c^2}\frac{1}{\exp(h\nu/kT)}\,. \quad \text{(1c)}$$

h is Planck's constant, and k is Boltzman's constant.

Scattering, although neglected here, may arise from liquid, ice, or melting liquid, depending on the size distribution of the particles. For simplicity of notation, we have suppressed the frequency dependence of τ and α in Equation (1). This equation and its Rayleigh-Jeans approximation are discussed in [25], and its more general form, including scattering, is discussed in [26]. For our purposes, we note the dependence on the temperature profile $T(s)$ and the implicit dependence on pressure, water vapor, and cloud liquid through $\alpha(s)$. For a plane-parallel atmosphere, the path length, s, and the height, h, are related by $s\sin(\theta) = h$, where θ is the elevation angle. Information on meteorological variables is obtained from measurements of T_b as a function of ν and/or θ. Equation (1) is used (a) in forward model studies in which the relevant meteorological variables are measured by radiosonde in situ soundings [27, 28, 29]; (b) in inverse problems and parameter-retrieval applications, in which meteorological information is inferred from measurements of T_b; and (c) in system modeling studies for determining the effects of instrument noise on retrievals and optimum measurement ordinates, such as ν and θ. Calculations of T_b for a warm (surface temperature T_s = 293 K) atmosphere are shown in Figure 2. We note the transmission windows near 30-50 GHz, 70-100 GHz, and 130-150 GHz. Radiometer measurements near these windows are used primarily for remote sensing of clouds and water vapor. The strong absorption features near 60 GHz and 118 GHz are used for temperature sensing. Finally, the strong absorption region near 183 GHz can be used to study very low amounts of water vapor [30].

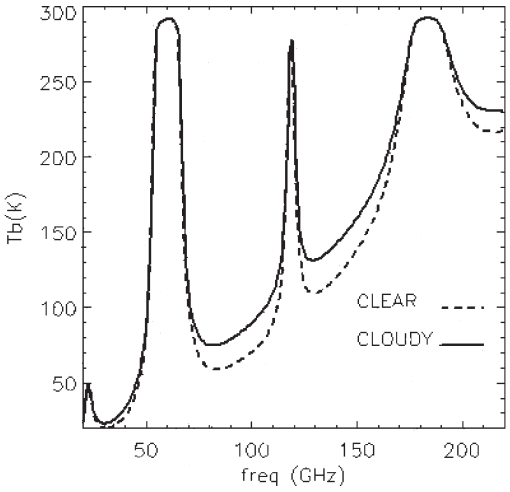

Figure 2. Calculated brightness temperatures (K) from 20 GHz to 220 GHz for clear and cloudy conditions. The clear calculations were based on a standard atmosphere with the surface values (S) of P_S = 1013 mb, T_S = 293 K, ρ_S = 10 gm^{-3}, and IWV = 2.34 cm. The cloudy atmosphere contained 1 mm of integrated cloud liquid with a cloud layer of liquid density of 0.1 gm-*3* between 1 and 2 km. The absorption models used are given in Figure 1.

3. Observation Techniques

Measuring downwelling thermal emission by microwave and millimeter-wavelength radiometers from a surface-based platform is now routinely performed on an operational basis [2, 3]. In addition, surface-based

radiometers are frequently deployed in campaigns specifically designed to study water vapor [29], clouds [31], and temperature [32, 33, 34]. In some deployments – specifically designed to measure water vapor and clouds in combination with other zenith-looking sensors – zenith observations are of primary interest. In others, particularly those used to measure boundary-layer temperature profiles, elevation-scanning radiometers are frequently used. More recently, radiometers scanning in both azimuth and elevation are also used to observe clouds [35].

The fundamentals of microwave radiometers are clearly discussed in [25, 36, 37]. Radiometers used to observe the atmosphere are comprised of a highly directional antenna and a sensitive receiver, followed by a detector unit and a data-acquisition system: a total system that requires calibration. In this section, we briefly discuss general techniques common to ground-based systems, and then give examples of contemporary radiometers.

3.1 Antennas

An antenna measures the antenna temperature, T_A, which is the integration over 4π steradians of the product of the angular distribution of brightness temperature and the power pattern of the antenna Usually, the antennas have symmetric beam patterns, with typical widths from 1° to 6°. Because most remote-sensing systems perform scanning in a vertical plane, low sidelobes are required to minimize contamination from ground emission. In addition, because surface-based antennas are deployed in rain and snow, protection from and reduction or elimination of environmental effects is of primary concern.

Perhaps the simplest antenna used to observe the atmosphere is a horn, either scalar or corrugated, that has a suitable beam pattern. If a multi-frequency and equal-beamwidth system is desired, the dimensions of the horns can be scaled appropriately. For some systems, the entire electronics package is rotated with the antenna. A more common system is to direct the antenna beam from the primary antenna onto a flat reflecting mirror that is scanned. In this configuration, only the flat reflector is moved. An example of this type of system is shown in Figure 3 [38]. Another common method is to use a lens antenna, which, again, views a flat reflector. More sophisticated scanning designs are also possible, such as the use of sub-reflectors, reflectors, and mirrors [35]. Frequently, the electronics package and the antenna are enclosed within a radome to protect the system from the environment.

During precipitation events, radiometer antennas/radomes usually get wet. One approach to reducing the effects of rain on a flat reflector was described by [39]. The reflector, when rotated rapidly, would quickly remove precipitation, although the reflector surface would accumulate a thin film of liquid. After a rain event, the reflector would dry within one to five minutes, and uncontaminated measurements could then be obtained. However, the measurements taken during rain were still contaminated. Hydrophobic coatings can reduce the amount of water drops on the radome surface [40], but this reduction is never complete. Blowers are useful to avoid the formation of dew on the microwave window, in particular when combined with heated air. Blowers are less effective for evaporation of raindrops, which was shown in the microwave radiometer inter-comparison campaign (MICAM) [41]. The time required to dry the radome after the rain event varied from a few minutes to several hours, depending on the radiometer design. For strong precipitation events, only the French DRAKKAR radiometer [41], which combines a small radiometer aperture with a strong blower system, needed less than an hour to dry. For larger systems, a shutter system controlled by a precipitation detector proved to be useful, as was done with the 22-channel radiometer MICCY (see Section 4.6), operated by the University of Bonn/Germany. One efficient way to allow measurements during precipitation is the observation at non-zenith elevation angles using a shelter protecting the instrument.

Another concern is the loss from dielectric lens antennas. Lenses for remote sensing are usually constructed from low-loss material (loss tangent less than ~ 10^{-3}). A lossy antenna attenuates an incoming signal and adds noise due to its own physical temperature. If the loss factor and the

Figure 3. The ASMUWARA in operation in Bern. The openings of the four horns appear as grey disks at the left of the rotatable mirror, while the IR radiometer looks through the white cylinder below the largest horn.

lens temperature are known, the unwanted signal can be corrected from the measured brightness temperature. The effect can be calibrated out by external targets or tipping curves (see Section 3.3.2), and a limitation is imposed by the time spent between valid calibration observations.

3.2 Receivers

A variety of receiver designs are also common in surface-based radiometry, and several involve Dicke modulation-type radiometers, in which the input to the receiver is alternatively switched between the scene (sky) and an internal calibration load [37]. In the original ETL design [1], the receiver was based on the Hach [42] design, in which the signal was sequentially switched between the scene and two internal blackbody targets (hot = 145° C and reference = 45° C). These targets were simply waveguide terminations kept at strictly controlled and measured temperatures. In the Radiometrics Corporation design (http://www.radiometrics.com), a signal generated by a noise diode is alternatively turned off and on and added to the signal from the scene at each angle, including the target. The Russian-designed scanning radiometers for boundary-layer temperature measurement [32, 33, 34] are total-power radiometers, but have been modified to include the signal from a noise generator. Both the NOAA/ETL Dual Channel radiometer (see Section 4.1) and the NOAA/ETL Ground-based Scanning Radiometer (see Section 4.9) receivers use either conventional Dicke or Hach switches that alternate between an internal reference load(s) and the scene. Finally, all of the above receivers are of double-sideband design, in which the signal from a stable local oscillator is mixed with the incoming radio-frequency signal emanating from the scene; the intermediate-frequency (IF) signal is then amplified and detected. With IF bandwidths usually around 500 MHz to 1 GHz, one-second radiometric sensitivities of 0.1 K are common. Also noteworthy is a specially constructed high-stability radiometer [43]. Based on typical analysis (see Section 3.3.3), this unit gave rms errors of less than 0.05 K over time periods of a month, and stabilities of better than 0.01 K over time scales of 1000 s to 10000 s. Another possibility is to use direct detection at the radio frequency of interest, thus eliminating the mixer and local oscillator. As improvements are made in radio-frequency amplifiers, increasing use of direct detection is expected. The use of Dicke or Hach switching overcomes the effect of receiver-gain variations, but can reduce the sensitivity of the receiver. As improvements are made in temperature and other environmental controls, total-power radiometers may become more common. Both MICCY (see Section 4.6) and RPG-HATPRO (see Section 4.7) illustrate some of these more recent developments.

3.3 Calibration

To derive quantitative information from radiometric measurements, accurate calibration is required, with accuracies of 0.5 K to 1.0 K. Most radiometric receivers have one or two internal noise sources that provide some measure of calibration. However, waveguide losses, lack of complete knowledge of radiometric parameters, and a host of other causes usually dictate that some external calibration method also be employed. We assume that the radiometer uses a square-law detector, in which the output voltage is proportional to the input power: i.e., voltage is proportional to the antenna temperature. We will briefly describe three commonly used calibration techniques.

3.3.1 External Blackbody Reference Targets

A seemingly straightforward calibration method is to view two external blackbody targets that are kept at two widely separated temperatures [37]. If T_1 and T_2 are the two target temperatures, with respective output voltages of v_2 and $v1$, then

$$\left(T_A\right)_S = T_1 + \frac{T_2 - T_1}{v_2 - v_1}\left(v_S - v_1\right), \qquad (2)$$

where $\left(T_A\right)_S$ is the antenna temperature of the scene and v_S is the corresponding voltage.

Preferably, the target temperatures bracket the range of antenna temperatures emitted from the scene. Also, it is important to construct targets with high emissivity such that reflections from external sources are negligible, and to have the targets sufficiently large that at least one and one-half to two projected antenna diameters are captured by the target system. Targets are frequently constructed with a surface having high thermal conductivity, covered with a thin layer of very absorbent material. Many times, a corrugated pyramidal surface, with wavelength-dependent spacing and depth ratios, is constructed to reduce reflections and hence to increase emissivity. The target is frequently embedded in a thermal insulator that is transparent to incoming radiation. Finally, when a target is placed in a thermal environment in which the environmental temperature differs greatly from the desired target temperature, measurements of target temperatures at several locations within the target are essential. The target calibration methods are most useful when the atmospheric brightness temperatures are within the range of easily achieved target temperatures: e.g., near the center of the 60 GHz O_2 absorption, or near the 183.31 GHz water-vapor line.

3.3.2 The Tipping-Curve Calibration Method

In the transmission windows from 20 GHz to 45 GHz or from 70 GHz to 150 GHz, clear-sky T_b values can be in the 10 K to 50 K range, and operational deployment of targets with temperatures that are in this range is difficult.

In this low transmission case, the so-called tipping-curve calibration method (tipcal) can give a high degree of accuracy [2, 44], and has been commonly used throughout the microwave community. In this method, brightness temperatures are measured as a function of elevation angle, θ, and are then converted to opacity, $\tau(\theta)$, using the mean radiating temperature approximation [45].

For each angle, an angularly-dependent mean radiating temperature, $T_{mr}(\theta)$, is used to derive the optical depth, $\tau(\theta)$, from

$$\tau(\theta) = \ln\left\{\frac{B_\nu\left[T_{mr}(\theta)\right] - B_\nu(T_c)}{B_\nu\left[T_{mr}(\theta)\right] - B_\nu\left[T_b(\theta)\right]}\right\}. \qquad (3)$$

If the system is in calibration, then the plot of $\tau(\theta)$ as a function of (normalized) air mass, m $(= \csc(\theta))$, will pass through the origin; conversely, if $\tau(m) = \tau(1)m + b$ does not pass through the origin, then a single parameter in the radiometer equation is adjusted until it does. Note that when the calibration is achieved, then the slope of the line is equal to the zenith opacity. Several of the factors affecting the accuracy of tipcals were analyzed in [44], and their major results are summarized below:

A. The effect of the refractive-index profile on system calibration is negligible, and the fact that the Earth's curvature has a relatively large effect that can be conveniently corrected to less than 0.05 K for air mass ≤ 4.
B. Pointing errors could have a serious impact on the performance of the tipcal if only one-sided scans are used. Experience and simulations strongly suggest that antenna scans used for calibration should be taken in pairs, at symmetric elevation angles.
C. A correction must be made when converting the antenna temperature $T_a(\theta)$ to $T_b(\theta)$. A correction based on half-power beamwidths was given in [44].
D. The quantity T_{mr} plays a role in mapping brightness temperature, T_b, to opacity, τ. Using a T_{mr} that is a function of elevation angle and is estimated by surface meteorological measurements is an effective way of reducing errors in T_{mr}. The prediction could also be improved significantly by using remote sensor observations [82].
E. The system random noise affects system precision, but with both the ETL and the ARM systems (rms noise ~ 0.1 K), the calibration uncertainties are about 0.1 K - 0.4 K. Reference [44] also found that the use of T_b at larger air masses suffers less than the use of T_b at smaller air masses due to a larger signal-to-noise ratio at lower elevation angles. The impact of the system noise can usually be reduced by temporal averaging.
F. Errors caused by uncertainty in the offset term of the radiometer equation will not cause serious calibration problems if the offset uncertainty is less than 1 K. See [44] for two common types of radiometer equations.
G. Errors caused by non-stratified atmospheric conditions are the most serious limitation for tipcal, and can occur due to clouds and horizontal variations in the water-vapor field. Various criteria based on symmetric scans are available to determine the quality of a tipcal [2, 44].

In summary, the tipcal method, when applicable, can give absolute accuracies of 0.3 K to 0.5 K rms.

3.3.3 Brightness Temperature Calculations to Calibrate

For a highly stable radiometer, such as the NOAA/ETL prototype [1] that was operated at a radiosonde launch facility, radiosonde data that are taken during clear-sky conditions can be used with a forward radiative transfer model, Equation (1), to calculate T_b values. If the T_b values are taken over a variety of elevation angles, or over a range of meteorological conditions, the measured data can be used as calibration points. This method implicitly assumes the correctness of the forward model and also of the radiosondes. The technique is most applicable near highly absorbing spectral regions, such as in the 60 GHz oxygen region, for which the calculated T_b values are insensitive to the choice of forward model. When applied to all channels of a multi-frequency radiometer that derives meteorological information, it also ensures internal consistency between radiometric data and the forward model used in retrievals.

4. Examples of Radiometric Systems

In this section, we discuss several types of contemporary ground-based radiometers. Since some of these are commercially available, we, of course, do not endorse any particular instrument.

4.1 NOAA/ETL Dual-Channel Radiometer

NOAA/ETL designed, constructed, and currently operates several dual-frequency radiometers at (20.6 GHz or 23.87 GHz, 31.65 GHz) that are used for measuring integrated water vapor (IWV) and liquid water path (LWP) [1]. For each of the radiometers, the electronics and the antenna and feed, are all housed in a benign environment, such as a seatainer. In this environment, the radiometer is free from precipitation, and the internal temperature of the seatainer is controlled to about 5°. The antenna is an offset paraboloid with a hybrid-mode feed, which results in high-quality radiation patterns that minimize the effect of extraneous sources of noise; the antenna aperture is devoid of blockage, and the beam is steerable in a vertical plane. The antenna has the same beamwidths at both frequencies (the full width at half power – FWHP – is either 2.5° or 4.0°), thus minimizing differential beam-filling during non-homogeneous cloud conditions. Some ETL systems have rapidly rotating reflectors to reduce the effects of rain [39]. The radiometer is triple switched in the Hach [42] mode; this results in continuous internal calibration and high stability. External calibration is accomplished on roughly a weekly basis using the tipcal method.

4.2 Radiometrics Corporation Microwave Radiometer (MWR)

Radiometrics Corporation has designed, constructed, and sold several dual-frequency (23.8 GHz and 31.4 GHz) MWRs for measuring integrated water vapor and liquid water path [2]. Each radiometer is easily portable, and all electronics, antenna, and calibration targets are enclosed in a radome. The antenna is a corrugated horn with a dielectric lens that views a stepping mirror, for scanning the atmosphere, and a blackbody target. The FWHP beamwidths of the system are 5.9° at 23.8 GHz and 4.5° at 31.4 GHz. The gain of the system is determined by viewing the target with and without noise injected by a noise diode. Calibration of the system consists of determining the effective noise-diode temperature, T_{ND} , and is done by the tipcal method. When tipcal can't be done, T_{ND} is estimated by a procedure described in [2]. The MWR is equipped with a heated blower and a moisture detector to minimize the effects of rain and dew.

4.3 Tropospheric Water Vapor Radiometer (TROWARA)

A first-generation radiometer system for continuous measurements of integrated water vapor and of liquid water path was operated at the Institute of Applied Physics (IAP) at the University of Bern. The instrument, called TROWARA, was designed and built at the IAP. It operated at 21 GHz and 31 GHz [46] with internal calibration, supplemented by hourly tipping curves [44, 47]. The limitation to two channels required an estimate of the effective tropospheric temperature [48]. TROWARA has provided a large data set over the years. Inter-comparisons of measured integrated water vapor with other remote-sensing methods and with nearby radiosonde data showed reasonable agreement, but at the same time, these revealed systematic differences on the order of 1 kg/m^2 [49, 50, 51]. A special test was the participation of TROWARA in the Cloud-Liquid Water Network (CLIWA-NET) [31]. Due to the failure of the 21 GHz channel during the first campaign, a method was developed to retrieve the required information by combining the 31 GHz radiation with Global Positioning System (GPS) data [38]. The instrumental degradation initiated a renovation and system reanalysis, leading to a new calibration model and the relocation from outdoor to indoor operation, viewing the sky through a Styrofoam window for enhanced stability [53]. In this way, TROWARA is able to observe downwelling brightness temperatures at an elevation angle of 40° under all weather conditions, including rain, since November, 2002. The data will form part of a database for climate research to be established within the project called "Studies in atmospheric radiative transfer and water-vapor effects," and is sponsored by the Swiss NCCR Climate Program (http://www.nccr-climate.unibe.ch/).

4.4 Meteorological Temperature Profiler MTP5

Kipp & Zonen BV is now marketing a radiometer that was originally designed and deployed by the Russian firm ATTEX [32, 34]. This radiometer is designed to measure temperature profiles in the boundary layer from 0 m to 600 m AGL. The radiometer is a single-channel (61 GHz) solid-state Dicke-type superheterodyne receiver that is electronically chopped at 1 KHz between the sky and a reference noise source. The antenna is a scalar horn with a FWHP beam width of 6°, and scans by viewing a flat reflector at each of 11 scanning angles. Because of the 2 GHz bandwidth and a low receiver noise temperature of 600 K, a high sensitivity of 0.04 K is achieved. Calibration of the receiver is achieved by 0.1° C temperature control and a switched internal noise generator. A one-point absolute calibration is achieved either by viewing an external target, or by knowing the emission temperature in the horizontal direction. A variation of this radiometer, developed at NOAA/ETL, scans continuously in a 360° vertical plane, and, in addition to temperature profiles, can also be used to measure air-sea temperature difference [54].

4.5 Radiometrics Corporation Microwave Profiler

Radiometrics Corporation has developed a multi-frequency microwave radiometer that is based on a highly stable, tunable, synthesized local oscillator in the receiver. This design overcomes errors caused by receiver frequency drift, while allowing observation of a large number of frequencies across wide tuning ranges. The total power receiver has a highly stable noise diode that is used as a gain reference. The radiometer observes atmospheric brightness temperatures in five frequency bands from 22 GHz to 30 GHz, and in seven bands from 51 GHz to 59 GHz [3, 55, 90]. It also measures zenith infrared temperature, surface temperature, humidity, and pressure. The radiometer has automated elevation- and azimuth-scanning capability, and the observation interval can be as short as several seconds. The instrument is relatively portable, with a volume of 0.12 m^3 and a weight of 32 kg.

4.6 Microwave Radiometer for Cloud Cartography (MICCY)

MICCY is a 22-channel radiometer operated by the University of Bonn [35]. It is capable of high temporal (0.1 s) and spatial (< 1°) resolution. The radiometer has 10 channels on the high-frequency side of the 22.235 GHz water-vapor line, 10 channels on the low-frequency side of the 60 GHz O_2 absorption ban, and two channels at 90 GHz. Both H and V polarization are measured at each frequency of operation. MICCY is a single-sideband total-power

radiometer that is based on a heterodyne receiver filter-bank design (parallel detection of all frequency channels). A Dicke modulation scheme is not foreseen for the system, since the thermal stability of the receivers is less than 20 mK, which implies that the instrument is capable of maintaining its radiometric accuracy for several minutes without recalibration. Both targets and inserted noise from highly stable diodes are used in calibration. With FWHP beam widths of about 0.9°, the radiometer is capable of full 360° scanning in azimuth and a zenith scan of 0° to 90°. The entire system can be scanned in azimuth and elevation for mapping of clouds. The latter is performed by a planar mirror that reflects the incoming radiation into a fixed 1 m Cassegrain system. The system comprises a quasi-optical multiplexer for three frequency bands. Internal ambient and cold blackbodies are used for absolute calibration, while internal noise calibration standards are used in between absolute calibrations. The entire system is mounted on a transportable trailer, and all parts are enclosed in a radome.

4.7 Radiometer Physics GmbH-Humidity and Temperature Profiler (RPG-HATPRO)

Because the implementation of an operational network of microwave radiometers is presently hampered by the cost and complexity of the available instruments, it was a major objective of the European CLIWA-NET project [31] to develop a network-suitable low-cost microwave radiometer. At first, the radiometer was only intended for the measurement of liquid water path, the key variable within CLIWA-NET. However, the design studies showed that a full profiling system, capable of simultaneous observation of liquid water path as well as temperature and humidity profiles, could be achieved for slightly higher costs. This radiometer – RPG-HATPRO – has been built by the German company Radiometer Physics GmbH (http://www.radiometer-physics.de/html/RPG_home.html). It fulfills the requirements defined within CLIWA-NET. For example, the maintenance interval is two months, the outside temperature range is from –30° C to +45° C, and the following features are available: rain detection and protection by a shutter system; GPS clock; measurements of environmental temperature, pressure, and humidity; possible Internet connection; and portability. The radiometer avoids lossy components, such as lenses, in the optical section. Instead, an off-axis paraboloid is used for both beam imaging and elevation scanning.

The RPG-HATPRO comprises total-power radiometers utilizing direct-detection receivers at all frequencies (14 channels up to 60 GHz). This approach avoids any problems that might arise from mixers or local oscillators (standing waves, frequency drifts, insufficient isolation, sideband suppression, higher system complexity, and cost). Thus, the stability and accuracy of the system are drastically improved. Furthermore, possible IF interference – caused, for example, by communication systems – is eliminated. The receivers of each frequency band are designed as filter banks in order to acquire each frequency channel in parallel. In addition, the flexibility to adjust each channel bandwidth individually allows for optimizing temperature profiling for both boundary layer and full troposphere.

4.8 All-Sky Multi-Wavelength Radiometer (ASMUWARA)

The ASMUWARA is a radiometer system designed for remote sensing of tropospheric water vapor, cloud liquid water, and temperature profiles [38]. It was designed and built at the IAP. The instrument consists of nine microwave channels in the frequency range from 18 GHz to 151 GHz; a broadband thermal infrared radiometer (wavelength band: 8 μm to 14 μm); meteorological sensors, including a rain detector; and an optional camera. The radiometers are housed in a temperature-controlled cylinder, with all beams aligned in a horizontal direction pointing to a rotating mirror that scans the sky and two calibration loads. The entire instrument can be rotated around its vertical axis. The beams perform a Rosetta-like pattern to map the sky hemisphere within 20 minutes. All channels

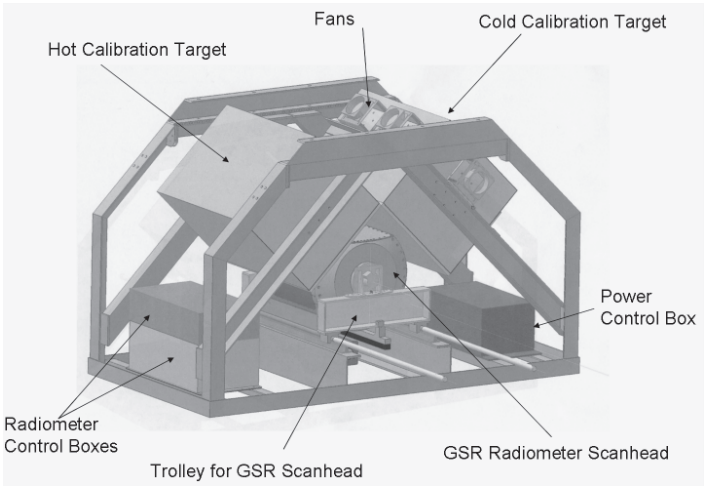

Figure 4. A schematic diagram of the GSR calibration and scanner system. The GSR scan head periodically moves out of the framework for atmospheric viewing on a trolley system, and shares time observing the atmosphere and the two thermally controlled blackbody reference targets.

have the same view and a common full beamwidth of 9°, formed by corrugated horns. The beamwidth is a compromise between angular resolution and sky coverage within the time scale of atmospheric variations. All horns are vertically polarized. The mirror reflection rotates the polarization during the scan from vertical, at the horizon, to horizontal, at nadir and zenith. A special challenge was the broad bandwidth required for the common instrument optics, ranging from 18 GHz to the thermal infrared. The solution was to construct a sufficiently large, flat aluminum mirror that allowed parallel beams for each spectral range, and to avoid any sort of radome. In this way, the instrument works well in periods without precipitation. A planned extension to all-weather operability will include a movable roof with a limited sky view during periods of rain. Figure 3 shows the weather-exposed parts of ASMURARA in operation on the roof at IAP. In principle, ASMUWARA is similar to other radiometer systems recently developed for the troposphere [3, 35. 90]. The main difference is the availability of and the concentration on the hemispheric imaging mode for all channels, including the infrared.

To avoid problems of internal calibration, two external calibration loads with good thermal properties were designed. In addition, tipcals are used for channels with low optical thickness. Whereas one load is kept as close as possible to the outside air temperature, the other load is warmer by about 10° C. Because of its favorable dielectric and thermal properties [56], beech wood was selected as the emitting material. A zigzag surface profile was selected to enhance the emissivity to at least 0.995 at all channels and at the relevant linear polarization. The temperatures of the loads are homogenized by internal ventilation, by a Styrofoam cover, and by monitoring with five thermocouples each.

4.9 NOAA/ETL Ground-Based Scanning Radiometer (GSR)

NOAA/ETL designed and constructed a multi-frequency scanning radiometer operating from 50 GHz to 380 GHz. The radiometers are installed into a scanning drum or scan head (see Figure 4). The GSR uses a sub-millimeter scan head with 11 channels in the 50-56 GHz region, a dual-polarization measurement at 89 GHz, seven channels around the 183.31 GHz water-vapor absorption line, a dual-polarized channel at 340 GHz, and three channels near 380.2 GHz. It also has a 10.6 μm infrared radiometer within the same scan head. All of the radiometers use lens antennas and view two external reference targets during the calibration cycle. In addition, the design of each of the radiometers includes two internal reference points for more-frequent calibration. The GSR instrument is a modification of a similar instrument that operated at the North Slope of Alaska/Adjacent Arctic Ocean site in 1999 [91]. A substantial improvement in radiometer calibration for ground observation in the Arctic environment has been achieved. Based on experience from the 1999 experiment, a new set of thermally stable calibration targets with high emission coefficients were also designed, constructed, and deployed. The primary use of the instrument is to measure temperature, water vapor, and clouds at cold ($-20°\,\mathrm{C}$ to $-55°\,\mathrm{C}$) and dry (PWV $< 5\,\mathrm{mm}$) conditions. A schematic of the GSR is shown in Figure 4. The beamwidths of the GSR channels are 1.8°, and can be averaged to give beamwidths that are consistent with the MWR (4.5° to 5.5°). The GSR was deployed in the NSA/AAO Arctic Winter Radiometric Experiment that was conducted in Barrow, Alaska, USA, during March-April, 2004 [92].

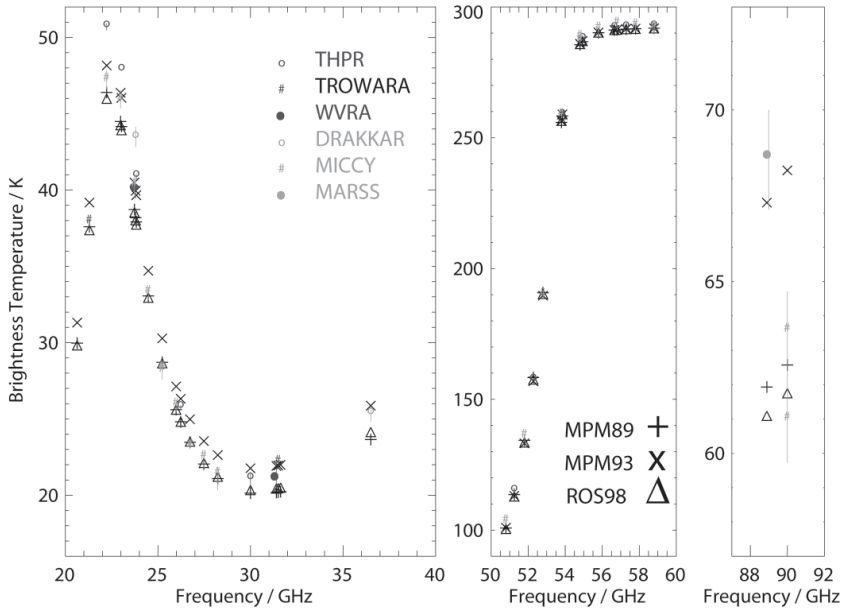

Figure 5. Simulated and measured brightness temperatures for a radio sounding on August, 2001, 11 UTC at Cabauw, the Netherlands. The radiometer measurements were averaged over 10 minutes past launch, and thin lines connect the maximum and minimum values within this interval. Simulations were performed using the gas absorption models MPM89 [4,13], MPM93 [14], and ROS98 [5].

4.10 Microwave Inter-Comparison Campaign

The Microwave Inter-Comparison Campaign (MICAM), during the first two weeks of August, 2001, comprised a unique comparison of eight microwave radiometers of different designs. It was performed at the central facility of the Dutch Weather Service (KNMI) in Cabauw, The Netherlands, where simultaneous measurements with cloud radar, ceilometer, radiosonde soundings, and many other instruments were performed. Most radiometers were already involved in the BALTEX Cloud Liquid Water Network, CLIWA-NET [31], at different locations within Europe. Thus, MICAM was intended to demonstrate that the measurements of the different radiometers were sufficiently comparable to be used to evaluate numerical weather prediction and climate models.

The radiometers were operated in Cabauw with a maximum separation distance of 30 m. In total, measurements at 47 different frequencies were performed. The observed brightness temperatures were compared with results from forward calculations based on high-quality radiosondes (RS-90). Meaningful comparisons can only be performed during cloud-free conditions, because it is not possible to model the liquid water content from radiosondes. Figure 5 shows one example for August 2, 2001. The spectral characteristics along the 22 GHz line and the 60 GHz oxygen complex are depicted well by the radiometers. Obviously, the 23.8 GHz channel of the DRAKKAR radiometer [31] overestimated the brightness temperature measured by three other radiometers (THPR [31], WVRA [31], MICCY [35]) at similar frequencies. A calibration problem has been identified by the responsible group (the French National Center for Scientific Research-CNRS), and a correction scheme has to be developed. The largest discrepancies between measurements occurred at 90 GHz. Unfortunately, the differences corresponded exactly to the uncertainties of the gas absorption models, and thus allowed no further constraint of these models. In conclusion, one can state that the accuracy of the raw brightness temperature measurements from the microwave radiometers is close to that of gaseous absorption models.

5. Retrieval Techniques

Techniques for deriving meteorological information from radiation measurements are generally based on Equation (1). Because only a finite number of imperfect radiation measurements are available, and a continuum of parameters is needed to describe profiles of temperature, water vapor, and cloud liquid, a rigorous mathematical solution does not exist, and the inverse problem is said to be ill-posed [57, 58]. Therefore, it is better to regard the measurements as constraints, and to blend them with supplementary sources of information or to drastically reduce the dimensionality of the inverse problem by projecting the profiles onto their linear functionals. Useful supplementary information can be provided by numerical meteorological forecasts, or by a priori information obtained from past data. Examples of profile linear functionals are integrated water vapor and liquid water path for moisture variables, and geopotential height for temperature profiles [45]. We briefly discuss algorithms that are commonly used in meteorological remote sensing.

Equation (1) can be approximated by a Fredholm integral equation of the first kind [9, 45]. In its discrete form it is written

$$g_e = Kf + \varepsilon , \tag{4}$$

where g_e is a vector composed of n measurements, f is an m-vector the components of which represent the profile that we want to determine, K is an $n \times m$ matrix relating the measurements to the unknown profile, and the n-vector ε explicitly denotes that the measurements have an unknown error component that will affect the solution to some degree. For mildly nonlinear problems, a perturbation form of Equation (1) is frequently used as the basis of subsequent iterations. Retrieval algorithms that require calculations of K for their implementation are called "physical." An excellent review article discussing techniques for solving Equation (4) was written by Rodgers [9].

A general algorithm for solving Equation (4) in the linear case is given by

$$\hat{f} - f_0 = \left[S_f^{-1} + K^T S_\varepsilon^{-1} K \right]^{-1} K^T S_\varepsilon^{-1} \left(g_e - K f_0 \right) . \tag{5}$$

This method is used to incorporate a priori statistics, including means and covariance matrices of f, S_f, and ε, S_ε, into the retrieval process [9, 45]. If successive approximations are used to generate Equations (4) and (5), then

$$\hat{g}_e = g_e - g\left(f_n \right) + K_n f_n , \quad n = 0,1,\ldots , \tag{6}$$

and

$$\hat{f}_{n+1} - f_0 = \left[S_f^{-1} + K_n^T S_\varepsilon^{-1} K_n \right]^{-1}$$

$$K_n^T S_\varepsilon^{-1} \left[g_e - g\left(f_n \right) + K_n \left(f_n - f_0 \right) \right] \tag{7}$$

In Equations (6) and (7), the matrices K_n are calculated for the nonlinear extension of Equation (4), using f_n as the expansion point for the required functional derivatives [9]. The matrices S_f and S_ε are defined as

$$S_f = E\{ f - f_0 \} \{ f - f_0 \}^T$$

and

$$S_\varepsilon = E\left\{\varepsilon\varepsilon^T\right\},$$

where the expectation value, E, ranges over a joint probability distribution of f and ε.

Choices of the function f_0 can include a climatological average, an initial guess based on a forecast, or an estimate derived from another remote sensor, and thus S_f is a measure of the uncertainty in the guess. In some cases the matrix could be diagonal, with $\left(\sigma_f\right)_i^2$ describing the uncertainty at the ith level, or even scalar, with $S_f = I\left(\sigma_f\right)^2$, were I is the identity matrix. Similarly, S_ε is composed of two terms: the first describes the instrumental uncertainty, and the second contains an estimate of the forward-model errors. If both S_f and S_ε are scalar, then the ratio $\gamma = (\sigma_\varepsilon)^2 \Big/ \left(\sigma_f\right)^2$ yields the regularization parameter γ of Twomey [57] and Tikonhov and Arsenin [58].

Although Equation (7) is general and many retrieval methods are its special cases, we mention a few other frequently used methods: neural-network inversion [59, 60], and Kalman filtering [61, 62, 63] and regression [64]. Kalman Filtering is also a general technique and is described in excellent books [65, 66]. Another technique of great promise is to combine radiometer data with a numerical forecast model, as has been done successfully in satellite meteorology [67, 68].

6. Radiometric Sensing of Tropospheric Meteorological Variables

Remote sensing of meteorological variables by radiometry is now a mature field, with a history of applications at least since the mid 1960s. The strengths of the techniques are accurate calibration, temporal resolutions of the order of seconds, and the ability to measure spatially integrated quantities. In this section, we review a few of the techniques that are now internationally well-established. We then present newer applications that have considerable potential for both research and operational meteorological applications.

6.1 Integrated Amounts of Water Vapor and Cloud Liquid

Both water vapor and cloud liquid are important variables in meteorology and climate. Due to thermodynamic processes of evaporation and condensation, as well as transport by winds, these quantities vary greatly in space and time. Water vapor is characterized by water-vapor density as a function of spatial coordinates and time. To characterize liquid in clouds requires knowledge of particle size, as well. Water clouds consist of a large number of droplets of varying sizes. The number of all droplets within the unit volume is the total number density [m^{-3}]. The drop-size distribution (DSD) describes the number density as a function of droplet radius, i.e., the number of drops per unit volume within a given radius interval. Due to the complex microphysical processes within clouds, drop-size distributions are highly variable in time and space. In contrast to raindrops, cloud droplets are perfect spheres. Thus, all cloud microphysical parameters can be calculated from the drop-size distribution. For example, the cloud liquid-water content (LWC) [kg m^{-3}] is given by the product of the total volume of water and the density of water. Because the volume of a sphere is proportional to the radius cubed, liquid-water content is also called the third moment of the drop-size distribution. It comprises one of the most interesting properties of clouds, and is the prognostic variable in most numerical weather-prediction and climate models for describing clouds, but few observations are available for the validation of the model results. By far the most accurate method for determining the liquid water path, the vertical integral of liquid water content, is ground-based passive microwave radiometry. However, for many applications it is also crucial to know at which altitudes the water is located. Several instruments can be used to determine the cloud-base height (e.g., cloud radars, cloud lidar ceilometers, and infrared (IR) radiometers); for cloud thickness, cloud radars are used. Finally, to determine profiles of liquid water content, the combination of passive microwave and cloud radar measurements is promising [69,70].

Dual-frequency measurements of brightness temperature at an optimum frequency near the 22.235 GHz water-vapor line and in a transmission window have been used to measure integrated water vapor and liquid water path for about 25 years [1, 45, 63]. The primary method is straightforward, and does not require the covariance matrices that are explicit in Equations (5) and (7). First, at each of the two frequencies, T_b is converted to opacity τ by use of Equation (3). The opacity, τ, is related to integrated water vapor and liquid water path, and to the dry component, τ_d, by

$$\tau = \tau_d + \kappa_V\left(IWV\right) + \kappa_L\left(LWP\right), \qquad (8)$$

where the mass absorption coefficients of water vapor, κ_V, and cloud liquid, κ_L, must be known.

In Equation (8), for example, we have

$$\kappa_V = \frac{\int_0^\infty \alpha_V\, ds}{\int_0^\infty \rho_V\, ds},$$

where α_V is the absorption coefficient due to water vapor and ρ_V is the water-vapor density. Using both a clear

and a cloud liquid-absorption model, together with an estimate of the atmospheric state (i.e., vertical profiles of pressure P; T; water-vapor density, ρ_V ; and cloud liquid density, ρ_L ;) the two mass absorption coefficients can be estimated. If the absorption models are accurate, then the accuracies of κ_V and κ_L are determined by the accuracy with which the atmospheric state is known. By solving the radiative-transfer equations at two frequencies, ν_1 and ν_2, for two unknowns, the integrated water vapor

$$IWV = \frac{\kappa_{L,\nu_2}\tau'_{\nu_1} - \kappa_{L,\nu_1}\tau'_{\nu_2}}{\kappa_{V,\nu_1}\kappa_{L,\nu_2} - \kappa_{V,\nu_2}\kappa_{L,\nu_1}}, \qquad (9)$$

and liquid water path,

$$LWP = \frac{-\kappa_{V,\nu_2}\tau'_{\nu_1} + \kappa_{V,\nu_1}\tau'_{\nu_2}}{\kappa_{V,\nu_1}\kappa_{L,\nu_2} - \kappa_{V,\nu_2}\kappa_{L,\nu_1}}, \qquad (10)$$

can be determined. The quantity τ' is $\tau - \tau_d$, where the total optical depth, τ, is determined from Equation (4). An example of integrated water vapor and liquid water path retrievals is shown in Figure 6. The general accuracy of dual-frequency radiometric measurement of integrated water vapor has been shown to be better than 1 mm rms [29]. However, because of the lack of in situ measurements of cloud liquid, an adequate experimental evaluation of liquid water path over a range of cloud conditions is not available.

Improvements on the dual-channel method can be made with multi-frequency observations. The liquid-water path can be estimated from atmospheric-emission measurements in the microwave region because in this spectral region the cloud contribution strongly increases with frequency (Figure 1). The standard dual-channel principle has been described above for the determination of integrated water vapor. For the retrieval of liquid water path, the channel close to the water-vapor absorption line corrects for the changing water-vapor concentration of the atmosphere. Such observations are – with the exception of expensive and rather limited aircraft measurements – the most accurate method for observing liquid water path with an estimated accuracy of better than 25 gm^{-2}. A rough estimation shows that about 10 gm^{-2} are caused by the measurement error, while the rest can be attributed to the under-determined retrieval problem. The additional use of the 90 GHz channel can further constrain the problem and improve accuracy to less than 15 gm^{-2} [69, 71].

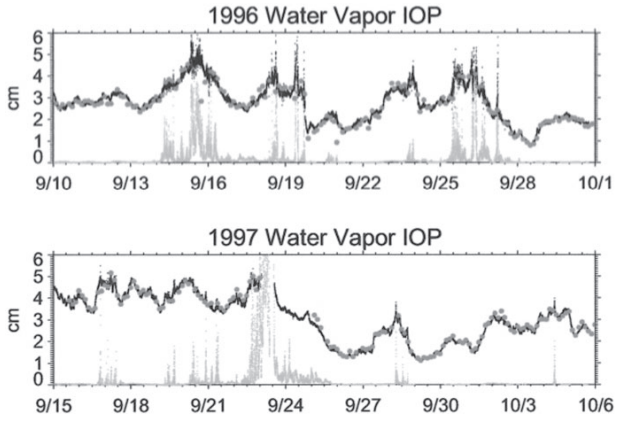

Figure 6. Precipitable water vapor and integrated cloud liquid (light solid line) derived from the NOAA/ETL microwave radiometer during the 1996 and 1997 Water Vapor Intensive Operating Periods. The circles represent PWV calculated from radiosonde profiles (after [29]).

6.2.1 Temperature Profiling

Radiometric temperature profiling can be accomplished by measuring the spectrum of radiation intensity at points along the side of the oxygen feature at 60 GHz [72]. By scanning outward from band center – where the opacity is so great that all signals originate from just above the antenna – onto the wing of the line – where the radiometer "sees" deeper (higher) into the atmosphere – altitude information is obtained. Emission at any altitude is proportional to local temperature; thus, the temperature profile can be retrieved. Either shoulder of the band center is suitable for retrieval of temperature-profile information.

A 6-channel zenith-viewing radiometer for measuring temperature was operated for several years by the NOAA Wave Propagation Laboratory (now the Environmental Technology Laboratory) [1]. The temperature-sensing channels of this radiometer were located at 52.8 GHz, 53.85 GHz, 55.45 GHz, and 58.8 GHz, and channels at 20.6 GHz and 31.65 GHz were used for measurement of water vapor and cloud liquid. The instrument was co-located with a radiosonde launch site, and its statistical accuracy was measured by comparisons with radiosondes taken twice per day. Retrievals of temperature were made every two minutes using Equation (4), with temperature covariance matrices evaluated from past radiosonde data. The rms accuracy of retrievals was generally better than 2 K rms from the surface to 500 mb. Radiometric retrievals are typically smoothed replicas of the sharp structure that is frequently exhibited by physical profiles; however, the integrals of these profiles used in deriving geopotential heights (the height of a given pressure level) were comparable in accuracy to those of radiosondes themselves. An example of geopotential height retrievals and comparisons with radiosondes is given in [45]. Radiometric temperature retrievals based on multi-channel data were also investigated in [63, 73, 74, 75].

Currently, Radiometrics Corporation has developed an advanced passive microwave radiometer based on a highly stable tunable synthesized local oscillator in the receiver. The radiometer observes atmospheric brightness temperatures in five frequency bands from 22 GHz to 30

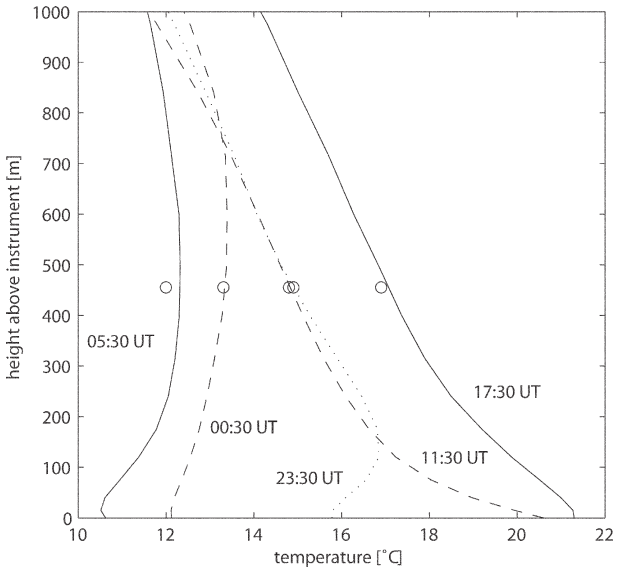

Figure 7. Temperature profiles in the lowest kilometer above ground at five different times on September 18, 2002, in Bern, measured with ASMUWARA, and a comparison with data from a meteo station (circles) located on a nearby TV tower (after [38]).

GHz, and in seven bands from 51 GHz to 59 GHz [3]. It also measures zenith infrared temperature, and surface temperature, humidity, and pressure. The radiometer has automated elevation and azimuth scanning capability, and the observation interval can be as short as several seconds. The instrument is relatively portable, with a volume of 0.12 m^3 and a weight of 32 kg. Historical radiosonde and neural network or regression methods are used for profile retrieval. Retrievals include temperature and humidity soundings up to 10 km height, and one-layer cloud liquid soundings.

Radiometric retrievals from this instrument are similar in accuracy to radiosonde soundings when used for numerical weather prediction [3]. Radiosonde assimilation errors used by the National Centers for Environmental Prediction for numerical weather analysis, and radiometric retrieval error determined from statistical comparisons with radiosondes [76], are of similar quality. Retrieval error is smaller than radiosonde sounding error for boundary-layer temperatures, and slightly higher above the boundary layer. The dominant radiosonde error is "representativeness" error. This results from the characterization of a model cell volume by a point measurement. This type of error is especially important when there are strong temporal or spatial gradients in the meteorological profiles. Radiometric retrievals are based on temporal averages, and are less susceptible to representativeness error than are radiosonde soundings. One of the potential advantages of high-temporal-resolution radiometric data (10 min to 15 min) is that the data could be directly assimilated into weather forecast models and improve short-term forecasts [76].

Temperature profiles have also been derived from the ASMUWARA [38]. The temperature profile is retrieved by optimal estimation, using Channels 5 through 8, using a climatology from radiosonde data, as described in [38, 77, 78]. Temperature profiles of September 18, 2002, are shown in Figure 7. The profiles nicely follow the temperature development measured at the meteorological station Bantiger on a nearby TV tower. At this early stage, the retrievals of temperature and of atmospheric water are independent. This works well for temperature profiles in the lowest km, where the 57 GHz channel is the dominant source of information. However, as shown in Figure 8, emission from clouds can compete with oxygen emission at the lower frequencies and, in this way, degrade the temperature retrieval. Therefore, in future applications of this instrument, the synergy of all channels is to be exploited.

6.2.2 Boundary-Layer Temperature Profiling

Angular techniques for measuring emission were developed by the ETL in the early 1970s [80], but due to mechanical simplicity, the zenith-viewing multi-spectral radiometers were chosen by ETL [1] as a component of a prototype remote-sensing system. However, in 1992, Russian scientists developed a scanning single-channel

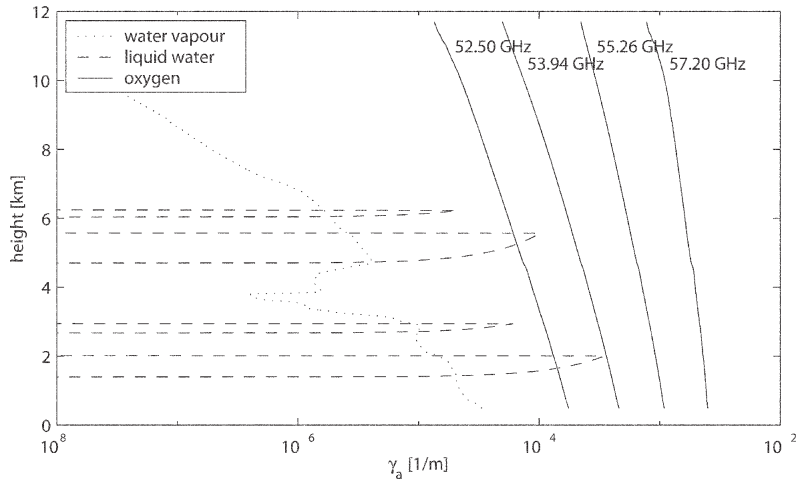

Figure 8. Vertical profiles of absorption coefficients due to oxygen of the temperature Channels 5 to 8 of ASMUWARA, and profiles of absorption coefficients at Channel 5 (52.5 GHz) due to water vapor and liquid water; simulations with MPM93 using radiosonde data from Payerne [38].

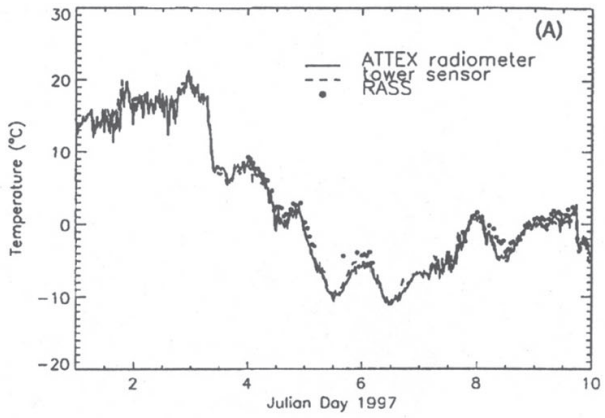

Figure 9a. A 10-day time series of temperature at 200 m as measured by the ATTEX radiometer, by the in situ measurement on the tower, and by a Radio Acoustic Sounding System (RASS) (January 1-10, 1997).

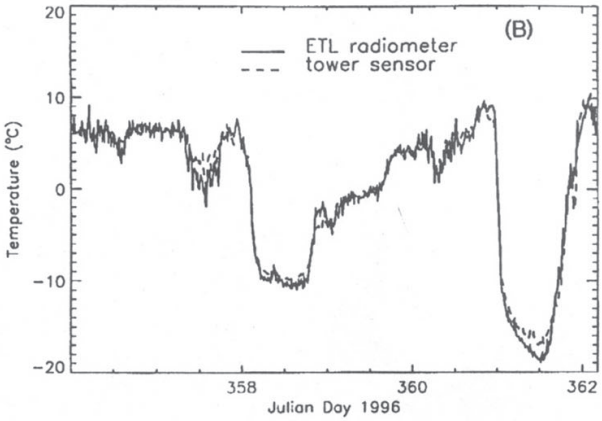

Figure 9b. A six-day time series of temperature at 200 m as measured by the ETL radiometer and by the in situ measurement on the tower (December 21-27, 1996; after [34]).

radiometer that showed promise for routine monitoring of the boundary layer [32, 73]. Development of this kind of radiometer has been continued by the Russian firm ATTEX, and numerous applications to boundary-layer studies have been published. The technique consists of measuring atmospheric emission at different angles in a wavelength band that exhibits relatively high atmospheric attenuation. The radiometer operates at 60 GHz (a wavelength of 5 mm), near the peak of the strong oxygen band; has a 6° beam width; and can yield data on a 1 sec basis. In this frequency region, the radiation in the horizontal direction can be used as a reference level, since it is essentially equal to the air temperature at the measurement height. Thus, an accurate air-temperature measurement provides a calibration of the radiometer offset. An independent measurement, such as a laboratory blackbody reference load, or calculations of T_b from radiosondes, is necessary to determine the radiometer's gain. Atmospheric air-temperature profiles can be obtained from the downwelling radiation at different elevation angles. The vertical resolution of the retrieved profiles is a function of altitude, and ranges from about 10 m near the surface to about 300 m at the 500 m altitude. Several experiments were conducted in Russia, Germany, the United Kingdom, and Japan by E. Kadygrov and his co-workers at ATTEX; a similar instrument has been operated by ETL near Boulder, Colorado, at a meteorological tower [81], at three experiments in Oklahoma, one in the tropics [28], and one at Barrow, Alaska [30]. In all cases, the rms errors were less than 0.5 K below 500 m. An example of temperature measured at 200 m above ground level (AGL) by the radiometer and by in situ measurements on a tower is shown in Figure 9. Because of the simplicity and portability of the instrument and its extremely flexible characteristics, it has been used from airborne, ship-, and ground-based platforms.

There also was a substantial amount of research into temperature profiling in particular, and microwave radiometry in general, in the former Soviet Union. A comprehensive review of this work, which contains numerous references to the original work, is contained in the book by Stepanenko et al. [89].

6.3 Profiling of Water Vapor

Information on the vertical distribution of water vapor is contained in the intensity and shape of the emission from pressure-broadened water-vapor lines. At high altitude, the emission from water vapor is from a narrow line, and at low altitudes, this line is pressure broadened. The intensity of emission is proportional to vapor density. Scanning the spectral profile and mathematically inverting the observed data can yield information on water-vapor profiles. Because of the relative weakness of the 22.235 GHz water-vapor line, frequency scanning of this line can yield only limited information on the vertical structure of profiles. In the clear troposphere, out of a possible selection of many frequencies around the 22.235 GHz line, only two or three channels are independent within radiometric noise levels of 0.5 K rms. However, because of the radiometric accuracy of better than 0.5 K that can be achieved by tipcal during clear conditions [44], it is promising that three well-calibrated measurements could have an impact on short-term moisture forecasts.

When radiometric data are accompanied by measurements from active sensors, such as cloud radars or lidars [8], added constraints can be imposed on the derived vapor profile [93]. For example, if the lower and upper boundary of a liquid cloud is known, then within the cloud layer, the relative humidity is 100%. If, in addition, information is known about the temperature profile, then the absolute humidity within the cloud layer is also known. Other synergies between radiometers and radars are also promising [82, 83].

The water-vapor line at 183.31 GHz is used for vapor profiling from aircraft and from satellites [52]. From a airborne platform, the high opacity of this line makes it ideal for lower-stratosphere and upper-troposphere water-vapor sensing. When used from a surface-based platform and for integrated water vapor amounts greater than about 5 mm, radiometric measurements in the vicinity of this line are

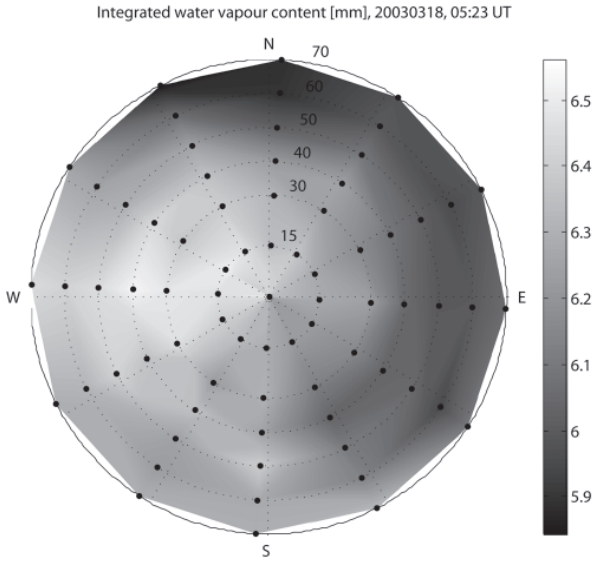

Figure 10. The hemispheric integrated water vapor distribution above Bern on March 18, 2003, as derived from ASMUWARA (after [38]).

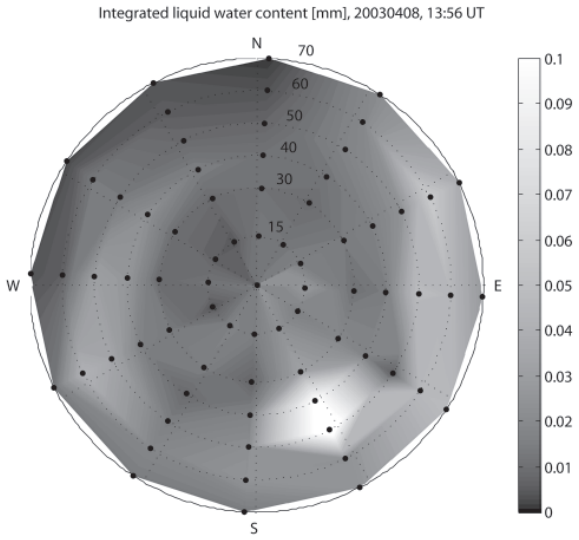

Figure 11. The hemispheric integrated liquid water distribution above Bern at 13:56 on April 8, 2003, as derived from ASMUWARA (after [38])

near saturation, and yield little information about moisture. However, during arctic winter conditions, when temperatures are frequently less than $-20°$ C and integrated water vapor is less than 2 mm, information on water-vapor structure and integrated water vapor can be obtained from multi-frequency measurements near the line [30].

6.4 Angular Scanning Observations of Cloud Liquid

As discussed in Section 4.8, the ASUMUWARA is capable of hemispheric imaging of clouds and water vapor. For channels with optically thin radiation, measured T_b can be accurately converted to opacity, τ. In turn, equivalent zenith values of integrated water vapor and liquid water path can be derived from τ. Based on local climatology and simulations based on MPM-93 [14], regression coefficients relating τ at 23.6 and 31.4 GHz to integrated water vapor and liquid water path were derived and applied to angular scanning data. An example of a hemispheric integrated water vapor image is shown in Figure 10; a spatial water-vapor variation appears with a gradient from northeast to southwest. A snapshot of the partly cloudy sky is depicted by the liquid water path data derived from channels 3 and 4 (Figure 11) and simultaneously by the thermal IR brightness temperature, T_{IR} (Figure 12). Clear sky is represented by $LWP = 0$ and T_{IR} below $-50°$ C. Liquid-water clouds with liquid water path up to 0.1 kg/m^2 and $T_{IR} \cong -25°$ C are apparent. For data evaluation, Martin et al. [38] compared integrated water vapor values in the range from 2 to 12 kg/m^2 from ASMUWARA with radiosonde data during the first winter period. The radiosonde values were slightly higher (bias 0.8 kg/m^2), whereas the standard deviation was 0.6 kg/m^2. Part of the bias was explained by the lower altitude of the Payerne station.

While the ASUMUWARA antenna beamwidth and scan patterns are optimized to provide a fast overview of the entire hemisphere, small-scale information on the cloud structure is measured by the microwave radiometer for cloud cartography (MICCY; see Section 4.6) [35]. This radiometer makes scanning measurements with high temporal (0.1 s) and angular (less than 1°) resolution. Figure 13 shows several azimuth scans observed by MICCY, made at an elevation angle of 30°.

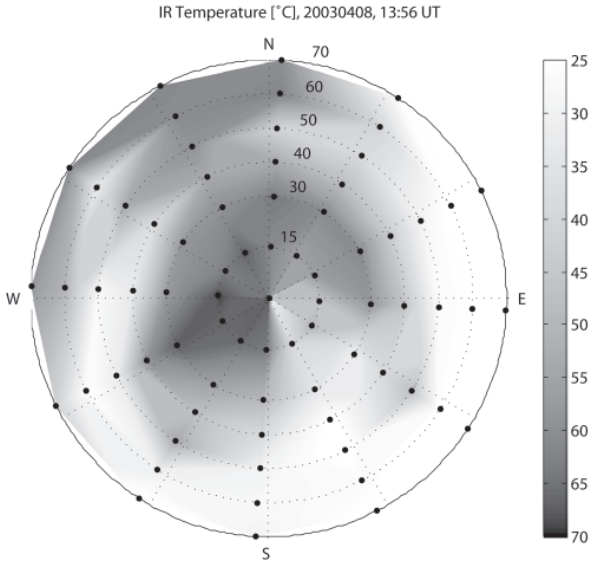

Figure 12. The hemispheric thermal IR image above Bern at 13:56 on April 8, 2003, as derived from ASMUWARA (after [38]).

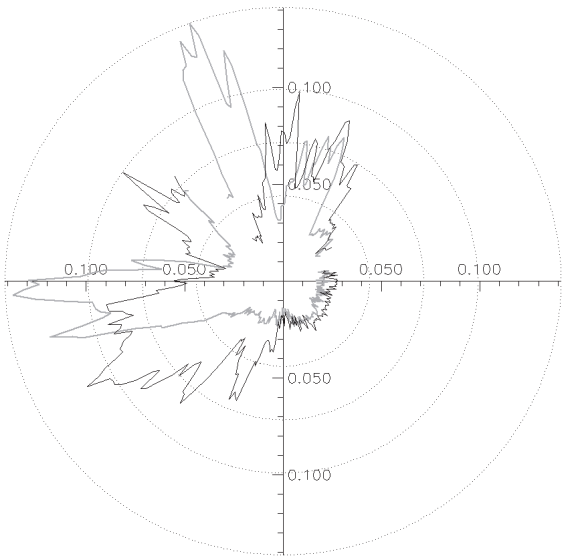

Figure 13 Series of 14 successive azimuth scans at 30 deg elevation with the multi-channel microwave radiometer MICCY having a beam width of less than 1 deg in all channels. Liquid water path was derived using a regression algorithm employing four frequency channels. After [69].

Such information can be used for studies concerning three-dimensional radiative transfer of solar radiation through clouds. Scanning measurements improve our estimate of the cloud water distribution and the cloud structure. Time series of cloud liquid water are strongly correlated on all spatial and temporal scales. Thus, for measurements in a fixed direction, it normally does not make sense to measure faster than once per second; this would only mean that you are measuring the same volume multiple times. By scanning, a new cloud volume is observed every time. Furthermore, by scanning the measurements are much better decorrelated, because the average distance between two points will be larger. Thus, a more representative, broader cloud water distribution will be found.

To extract cloud structure information from a large set of scans of liquid water path, we used the binned autocorrelation function, i.e., the correlation for all pairs of measurements within a certain range of distances (bin) was calculated and this was repeated for all bins. The correlation length (the length at which the autocorrelation function decreases below a threshold) is a strong function of the elevation angle: in one case study, the measurements made at an elevation of 43° were found to have a correlation length that is about three times as long as the correlation length at 70°. This is caused by the larger integration volume and, especially, the longer integration path of the measurements at 43°.

Scanning is important for studying the anisotropy of cloud structure. The binned autocorrelation can also be calculated for bins with a certain range of distances and angles to get a two-dimensional autocorrelation function. Two case studies showed strong anisotropies in the liquid water path field oriented in the direction of the wind. Thus, zenith measurements of the clouds that drift by on the wind would show a correlation length that is not representative of the field.

6.5 Integrated Profiling by Sensor Synergy

While the cloud water column can be derived accurately from microwave radiometer measurements alone, the information about its vertical distribution is rather limited. Therefore, microwave radiometer measurements are often combined with simultaneous cloud radar observations, which provide the radar reflectivity factor, Z, with a vertical resolution of approximately 50-100 m. Since Z is proportional to the sixth moment of the drop-size distribution and the cloud liquid-water content is proportional to the third moment, a direct conversion of Z to liquid water content results in large errors. Thus, a common approach used by Frisch et al. [70] scales the radar reflectivity profile to the liquid water path. A more sophisticated, physically based technique combines the microwave brightness temperatures, the attenuation-corrected radar reflectivity profile, the lidar-ceilometer cloud base, ground temperature and humidity, and the nearest operational radiosonde profile within an optimal estimation retrieval. The Integrated Profiling Technique (IPT) [82] can simultaneously derive profiles of temperature, humidity, and liquid water content. The retrieved IPT profiles are characterized by their physical consistency with respect to the microwave radiometer and cloud radar measurements. Additional constraints guarantee a match with the ground-level measurements, saturation within the cloud boundaries, and statistical consistency with the radiosonde temperature and humidity profiles. Error covariances of all measurements are required, such that all constraints can be met within an iterative optimal estimation procedure. The solution is interpreted as a probability density, so that a retrieval error estimate is inherently given. A further advantage of the IPT is that – in contrast to the liquid water path scaling methods – the liquid water content profiles are independent of errors of a liquid water path algorithm.

Presently, the IPT has been developed only for cases when the radar reflectivity is solely caused by liquid-water drops. This means that the occurrence of mixed-phase clouds within the vertical column above the instruments will make application of the IPT impossible. However, the presence of pure ice clouds above one or more liquid cloud layers will not influence the IPT, because ice clouds do not contribute to the microwave signal in the frequency range below 90 GHz. Furthermore, insect- and precipitation-dominated radar pixels need to be removed. Thus, to be able to apply the IPT automatically, a cloud classification was developed that distinguishes among six phases/regimes (pure ice, mixed-phase, pure liquid water, drizzle, significant precipitation, and unclassified). The classification makes

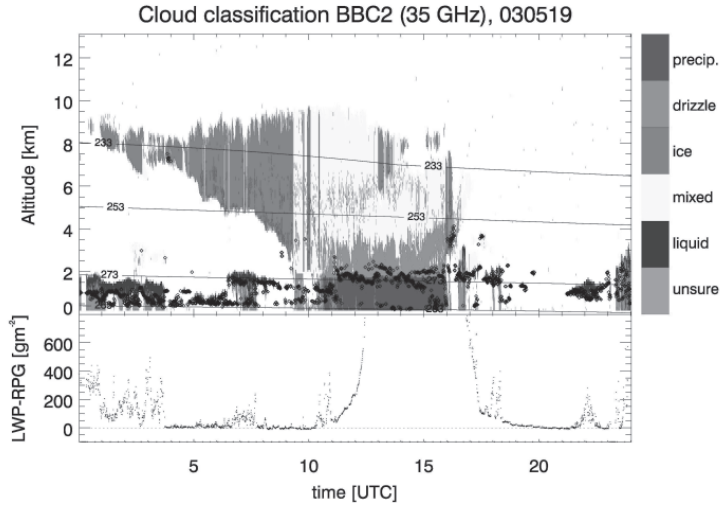

Figure 14. Cloud classification and liquid water path for May 19, 2003, at Cabauw. The temperature was derived from interpolated radiosondes. The classification was performed for each individual cloud radar range gate. The black dots indicate the cloud base height as observed by lidar ceilometer.

use of cloud radar, lidar-ceilometer, the nearest operational radiosonde temperature profiles, and microwave-radiometer-derived liquid water path. An example of the cloud classification for one day is shown in Figure 14. Obviously, the ice and mixed-phase clouds dominated the radar signal. Although the classification suggests that water clouds play a minor role, their strong influence on the solar radiation makes them of utmost importance for climate research. An IPT time series of liquid-water content, derived during the BBC2 campaign, is shown in Figure 15. Typical structures of a stratocumulus cloud can be observed with liquid water path values peaking around 400 g m^{-2}. The vertically integrated liquid water content values show quite good agreement with the liquid water path derived from a four-channel statistical retrieval.

The advantage of microwave remote sensing is that even in the presence of thick clouds, temperature and humidity can be determined with good accuracy. However, because the vertical resolution is relatively coarse (about 1-2 km [74]), sharp inversions can't be resolved completely. Figure 16 shows a time series of IPT-derived absolute humidity during the same time period shown in Figure 14. Again, quite good agreement of the integrated values can be seen between an independent statistical retrieval and the IPT. Notice the gradual increase of humidity as the cloudy period around 21.2 UTC sets in.

The IPT is a first step toward an "all-encompassing" profiling algorithm that combines measurements from all available instruments to derive the atmospheric state as accurately as possible. Since this task should ideally be accomplished in a physically consistent way, knowledge of all involved forward models is required. Future extensions will include infrared and ceilometer forward models to further constrain cloud microphysical parameters, especially in the lower part of the cloud.

7. Climate Applications

In the United States, the Department of Energy's Atmospheric Radiation Measurement (ARM) has developed a long-range program to study the effects of clouds on climate and on the development of climate models [84, 85]. In their experimental facilities to measure clouds and radiation, the ARM program has developed and operates three research sites in the Southern Great Plains (SGP), in North Central Oklahoma, USA, on the North Slope of Alaska (NSA), and in the tropical western Pacific (TWP). Because of their proven ability to measure integrated water vapor and liquid water path, ARM has deployed 10 MWRs (see Section 4.2) at their various research sites [2, 84]. The ARM facilities also routinely launch radiosondes, and

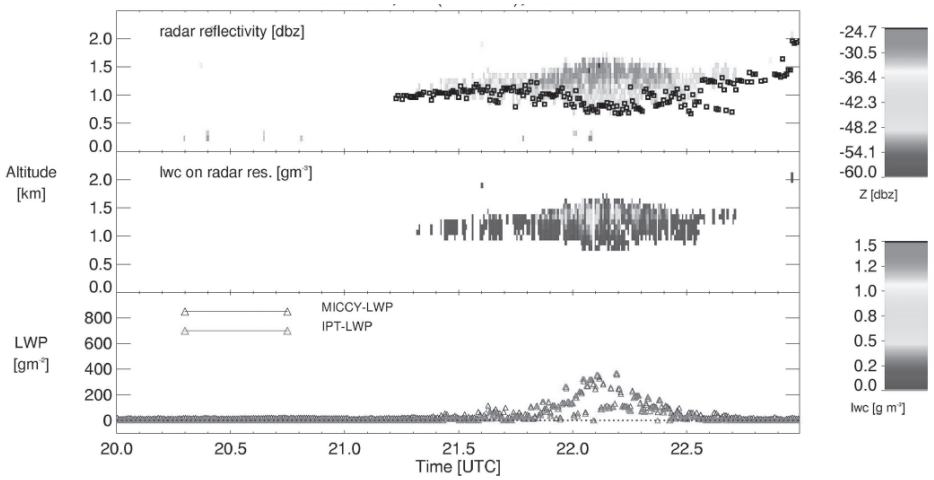

Figure 15. The radar reflectivity observed by a 35 GHz radar (top), the liquid water content retrieved using the integrated profiling technique (center), and the liquid water path (bottom), for the time period marked in Figure 14. The liquid water path was derived as the integral of the liquid water content values, and independently via a statistical algorithm from the set of brightness temperatures measured at four different frequencies.

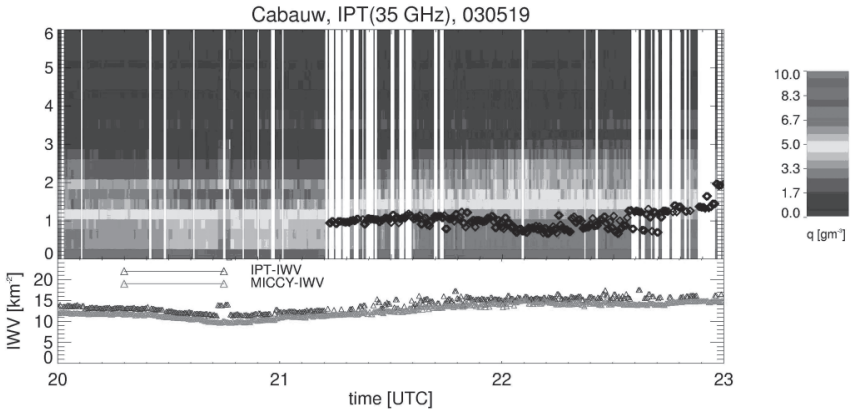

Figure 16. The time series of the specific humidity and integrated water vapor (IWV) for the same time interval as in Figure 14. The integrated water vapor was derived as the integral of the absolute humidity (q) values, and independently via a statistical algorithm from the set of brightness temperatures measured at four different frequencies.

operate infrared and optical radiation sensors, and lidar and millimeter-wave cloud radars (MMCR). In addition to providing measurement tools valuable for climate research, many of the data can be used to develop combined-sensor meteorological products.

One of the important results of MWR deployment has been the discovery and correction of dry bias humidity errors in Väisäla RS80 humidity sensors [7, 28]. The errors were first discovered in the comparison of measurements and radiosonde-based calculations of infrared radiance; consequently, three Water Vapor Intensive Operating Periods (WVIOPs) were conducted at the SGP [29] to address the problem. Several MWRs from a variety of US research institutions were deployed, and many kinds of radiosonde inter-comparisons were also done. As a result of these Water Vapor Intensive Operating Periods, currently, at the SGP site, all radiosondes are currently scaled by MWR integrated water vapor measurements. An example of the need for radiosonde corrections is shown in Figure 17, in which comparisons of calculations and MWR measurements are given. In this case, the use of an uncorrected radiosonde gave rise to a calculation error of about 10 K.

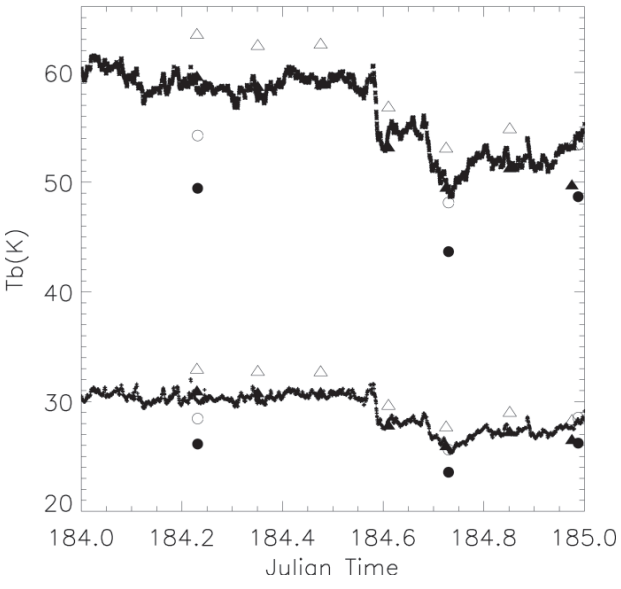

Figure 17. The 24-hr time series of T_b at 23.8 GHz (*) and 31.4 GHz (+) on July 3, 1999. The closed circles were calculated from the original ARCS-2 radiosondes (age = 315 days). The open circles were calculated from corrected ARCS-2 radiosondes. The closed triangles were calculated from the original RHB radiosondes (age = 172 days). The open triangles were calculated from corrected RHB radiosondes. The RTE model [5] was used (after [28]).

One possible limitation of MWR integrated water vapor measurements occurs during the arctic winter, when the integrated water vapor frequently is less than 2 mm, and the MWR lacks the sensitivity to provide accurate measurements. To overcome this limitation, radiometer measurements near 183 GHz have been made during cold and dry arctic conditions [30]. For example, during an entire month of cloud-free conditions at the NSA research site, the peak-to-peak variation of 23.8 GHz T_b was 3 K, while that from a millimeter-wave measurement at 183.31 ± 7 GHz was more than 80 K. An ETL/ARM experiment was conducted during March-April, 2004, to deploy a suite of radiometers ranging from 20 GHz to 380 GHz [92]. These instruments included the MWR, the Radiometric Profiler, and the GSR. Finally, this higher frequency is of great value not only for arctic regions, but also for mountain sites [79]. After instrumental improvements were completed, continuous observations at 183 GHz started again in early 2004 at the Jungfraujoch test site, at an altitude of 3600 m above sea level. About once every year, the radiometer-spectrometer instrument is also used in flight campaigns to measure the latitudinal variation of water vapor profiles in the stratosphere.

The MWR retrievals of liquid water path are also useful in developing models to calculate the transfer of solar radiation through clouds containing liquid, including mixed-phase clouds [86]. In particular, when MMCR and MWR are both available, the information on particle-size distribution can also be derived [87]. It is apparent that for years to come, the MWR will provide useful data for studying radiative transfer through clouds. For the cold arctic conditions, observations above 90 GHz can also improve cloud liquid retrievals.

8. Outlook

For the past 35 years, surface-based microwave radiometers operating below 60 GHz have provided useful data on temperature, water vapor, and clouds. Steady progress has been made in the development of robust, sensitive, and accurate radiometers. This has been accompanied by continued development of forward models for the accurate calculation of brightness temperature, although there is still some concern about cloud liquid characterization below freezing temperatures. The development of suitable inverse models has also occurred, but it now seems likely that assimilation of data with forecast models is the most promising technique for exploiting radiometer data [67, 68]. Of equal promise is the synergism of active and passive sensors, as has been achieved in cloud sensing [69, 70, 71], in moisture profiling [88, 89], and in the use of wind profiler estimates of significant moisture gradients to improve humidity profile retrieval [83].

Another promising area of research is the development of scanning radiometers that can measure horizontal gradients in water vapor and cloud liquid. For example, moisture gradients are frequently seen in tipcal measurements by MWRs [44].

The ASMUWARA has the potential to be an important tool for ground-based remote sensing of the troposphere. Advancements are expected to be made from the participation at the COST-720 inter-comparison campaign for temperature, humidity, and cloud profiling that was made in Payerne (Switzerland) from November, 2003, to January, 2004. Improvements will include the synergy of all channels in a coherent retrieval. With respect to instrumentation of ASMUWARA, an advancement will be the addition of the 151 GHz channel, which will allow higher sensitivity to clouds. Also to be exploited is the potential to measure precipitation; for this purpose, use will be made of the lower frequency channels (1 to 4) in case of rain, and the 151 GHz channel for dry snow. If the methods are successful, ASMUWARA will become a valuable tool in the ground validation of the international Global Precipitation Mission to be created by the space agencies of Europe, Japan and the USA. On the practical side, main improvements are expected from the protection of the instrument against wetting by raindrops.

Finally, the sensitivity of radiometers to both water vapor and cloud liquid increases with frequency, and arctic regions, with typical small amounts of both liquid and vapor, seem especially amenable to millimeter-wave radiometry. As satellite sensors increasingly use millimeter-wavelength radiometers, accurate forward models can be developed by using data from upward-looking sensors coupled with radiosondes. Such forward models are important in surface-, airborne-, and satellite-based remote sensing, as well as for communication.

9. Acknowledgements

We thank Ulrich Löhnert and Victor Venema for the fruitful discussions and the provision of figures. We thank Wim Hovius for his perfect management of the Cabauw observation site. Part of this work was done within the CLIWA-NET project sponsored by the EU under contract number EVK2CT-1999-00007. The algorithm development was partly funded by the German Department of Research and Education under Grant 07 AK106/0. A portion of the work presented in this paper was sponsored by the Environmental Sciences Division of the Department of Energy as a part of their Atmospheric Radiation Measurement Program. We thank Reginald Hill and Sergei Matrosov for several useful suggestions. We also thank Vinia Mattioli for her help in reformatting of several figures.

10. References

1. D. C. Hogg, M. T. Decker, F. O. Guiraud, K. B. Earnshaw, D. A. Merritt, K. P. Moran, W. B. Sweezy, R. G. Strauch, E. R. Westwater, and C. G. Little, "An Automatic Profiler of the Temperature, Wind and Humidity in the Troposphere," *Journal of Applied Meteorology*, **22**, 5, 1983, pp. 807-831.

2. J. C. Liljegren, "Automatic Self-Calibration of ARM Microwave Radiometers," in P. Pampaloni and S. Paloscia, (eds.), *Microwave Radiometry and Remote Sensing of the Earth's Surface and Atmosphere*, Utrecht, VSP Press, 2000, pp. 433-441.

3. R. Ware, R. Carpenter, J. Güldner, J. Liljegren, T. Nehrkorn, F. Solheim, and F. Vandenberghe, "A Multi-Channel Radiometric Profiler of Temperature, Humidity and Cloud Liquid," *Radio Science*, **38**, 4, 2003, pp. 8079-8032.

4. H. J. Liebe, "MPM, An Atmospheric Millimeter Wave Propagation Model," *International Journal of Infrared and Millimeter Waves*, **10**, 6, 1989, pp. 631-650.

5a. P. W. Rosenkranz, "Water Vapor Microwave Continuum Absorption: A Comparison of Measurements and Models," *Radio Science,* **33**, 4, 1998, pp. 919-928.

5b. P. W. Rosenkranz, "Correction to 'Water Vapor Microwave Continuum Absorption: A Comparison of Measurements and Models'," *Radio Science*, **34**, 4, 1999, p. 1025.

6. H. J. Liebe, G. A. Hufford, and T. Manabe, "A Model for the Complex Permittivity of Water at Frequencies below 1 THz," *International Journal of Infrared and Millimeter Waves*, **12**, 7, 1991, pp. 659-675.

7. D. Turner, B. Lesht, A. Clough, J. Liljegren, H. Revercomb and D. Tobin, "Dry Bias and Variability in Väisälä RS80-H Radiosondes: The ARM Experience," *Journal of Atmospheric and Oceanic Technology,* **20**, 1, 2003, pp. 117-132.

8. E. E. Clothiaux, T. P. Ackerman, G. G. Mace, K. P. Moran, R. T. Marchand, M. A. Miller, and B. E. Martner, "Objective Determination of Cloud Heights and Radar Reflectivities Using a Combination of Active Remote Sensors at the ARM CART Sites," *Journal of Applied Meteorology*, **39**, 5, 2000, pp. 645-665.

9. C. D. Rodgers, "Retrieval of Atmospheric Temperature and Composition from Remote Measurements of Thermal Radiation," *Reviews of Geophysics and Space Physics,* **14**, 1976, pp. 609-624.

10. Y. Han, E. R. Westwater, and R. A. Ferrare, "Applications of Kalman Filtering to Derive Water Vapor from Raman Lidar and Microwave Radiometers," *Journal of Atmospheric and Oceanic Technology*, **14**, 3, 1997, pp. 480-487.

11. M. Klein and A. J. Gasiewski, "Nadir Sensitivity of Passive Millimeter and Submillimeter Wave Channels to Clear Air Temperature and Water Vapor Variations," *Journal of Geophysical Research,* **105**, D13, 2000, pp. 17481-17511.

12. P. W. Rosenkranz, "Absorption of Microwaves by Atmospheric Gases," in Michael A. Janssen (ed.), *Atmospheric Remote Sensing by Microwave Radiometry*, New York, J. Wiley & Sons, Inc., 1993, Chapter 2, pp. 37-90.

13. H. J. Liebe and D. H. Layton, "Millimeter Wave Properties of the Atmosphere: Laboratory Studies and Propagation Modeling," National Telecommunications and Information Administration (NTIA) Report 87-24, 1987, 74 pp. (available from the National Technical Information Service, 5285 Port Royal Road, Springfield, VA, 22161 USA).

14. H. J. Liebe, G. A. Hufford, and M. G. Cotton, "Propagation Modeling of Moist Air and Suspended Water/Ice Particles at Frequencies below 1000," in *AGARD Conference Proceedings 542, Atmospheric Propagation Effects through Natural and Man-Made Obscurants for Visible through MM-Wave Radiation*, 1993, pp. 3.1 to 3.10 (available from NASA Center for Aerospace Information, Linthicum Heights, MD, USA).

15. H. C. Van de Hulst, *Light Scattering by Small Particles*, New York, Dover Publications Inc., 1981.

16. D. Deirmendjian, *Electromagnetic Scattering on Spherical Polydispersions*, New York, American Elsevier Publishing Company, Inc., 1969.

17. C. F. Bohren and D. R. Huffman, *Absorption and Scattering of Light by Small Particles*, New York, John Wiley, 1983.

18. P. Debye, *Polar Molecules*, New York, Dover, 1929.

19. E. H. Grant, J. Buchanan, and H. F. Cook, "Dielectric Behavior of Water at Microwave Frequencies," *Journal of Chemical Physics,* **26**, 1957, pp. 156-161.

20. V. I. Rosenberg, *Scattering and Extinction of Electromagnetic Radiation by Atmospheric Particles*, Leningrad, Gidrometeoizdat, 1972 (in Russian).

21. E. R. Westwater, Y. Han, M. D. Shupe, and S. Y. Matrosov, "Analysis of Integrated Cloud Liquid and Precipitable Water Vapor Retrievals from Microwave Radiometers during SHEBA," *Journal of Geophysical Research*, **106**, 23, 2001, pp. 32019-32030.

22. R. Rasmussen, R., M. Politovich, J. Marwitz, W. Sand, J. McGinley, J. Smart, R. Pielke, S. Rutledge, D. Wesley, G. Strossmeister, B. Bernstein, K. Elmore, N. Powell, E. Westwater, B. Stankov, and D. Burrows, "Winter Icing and Storms Project (WISP)," *Bulletin of the American Meteorological Society*, **73**, 7, 1992, pp. 951-974.

23. G. Hufford, "A Model for the Complex Permittivity of Ice at Frequencies below 1 THz," *International Journal of Infrared and Millimeter Waves*, **12**, 1991, pp. 677-682.

24. C. Mätzler, "Microwave Properties of Ice and Snow," in B. Schmitt et al. (eds.), *Solar System Ices, Astrophysical and Space Science Library,* **227**, Dordrecht, Kluwer Academic Publishers, 1998, pp. 241-257.

25. M. A. Janssen, "An Introduction to the Passive Remote Sensing of Atmospheres," in Michael A. Janssen (ed.), *Atmospheric Remote Sensing by Microwave Radiometry*, New York, J. Wiley & Sons, Inc,. 1993, pp. 1-36.

26. A. J. Gasiewski, "Microwave Radiative Transfer in Hydrometeors," in Michael A. Janssen (ed.), *Atmospheric Remote Sensing by Microwave Radiometry*, New York, J. Wiley & Sons, Inc., 1993, pp. 91-144.

27. S. Cruz Pol and C. S. Ruf, "Improved 20- to 32- GHz Atmospheric Absorption Model," *Radio Science*, **33**, 9, 1998, pp. 1319-1333.

28. E. R. Westwater, B. Boba Stankov, D. Cimini, Y. Han, J. A. Shaw, B. M. Lesht, and C. N. Long, "Radiosonde Humidity Soundings and Microwave Radiometers during Nauru99," *Journal of Atmospheric and Oceanic Technology*, **20**, 7, 2003, pp. 953-971.

29. H. E. Revercomb, H. E., D. D. Turner, D. C. Tobin, R. O. Knuteson, W. F. Feltz, J. Bannard, J. Bosenberg, S. Clough, D. Cook, R. Ferrare, J. Goldsmith, S. Gutman, R. Halthorne, B. Lesht, J. Liljegren, H. Linne, J. Michalsky, V. Morris, W. Porch, S. Richardson, B. Schmid, M. Splitt, T. Van Hove, E. Westwater, and D. Whiteman, "The ARM Program's Water Vapor Intensive Observation Periods: Overview, Initial Accomplishments, and Future Challenges," *Bulletin of the American Meteorological Society*, **84**, 1, 2003, pp. 217-236.

30. P. E. Racette, E. R. Westwater, Y. Han, A. J. Gasiewski, M. Klein, D. Cimini, D. C. Jones, W. Manning, E. J. Kim, J. R. Wang, V. Leuski, and P. Kiedron, "Measurement of Low Amounts of Precipitable Water Vapor Using Ground-Based Millimeterwave Radiometry," submitted to *Journal of Atmospheric and Oceanic Technology*, 2004.

31. S. Crewell, M. Drusch, E. van Meijgaard, and A. van Lammeren, "Cloud Observations and Modeling within the European BALTEX Cloud Liquid Water Network," *Boreal Environmental Research,* **7**, 2002, pp. 235-245.

32. E. N. Kadygrov and D. R. Pick, "The Potential Performance of an Angular Scanning Single Channel Microwave Radiometer and some Comparisons with In Situ Observations," *Meteorological Applications, UK*, **5**, 1998, pp. 393-404.

33. Y. G. Trokhimovski, E. R. Westwater, Y. Han, and V. Ye. Leuskiy, "The Results of Air and Sea Surface Temperature Measurements Using a 60 GHz Microwave Rotating Radiometer," *IEEE Transactions on Geoscience and Remote Sensing*, **GRS-36**, 1, 1998, pp. 3-15.

34. E. R. Westwater, Y. Han, V. G. Irisov, V. Leuskiy, E. N. Kadygrov, and S. A. Viazankin "Remote Sensing of Boundary-Layer Temperature Profiles by a Scanning 5-mm Microwave Radiometer and RASS: Comparison Experiment," *Journal of Atmospheric and Oceanic Technology*, **16**, 7, 1999, pp. 805-818.

35. S. Crewell, H. Czekala, U. Löhnert, C. Simmer, Th. Rose, R. Zimmermann, and R. Zimmermann, "Microwave Radiometer for Cloud Carthography: A 22-Channel Ground-Based Microwave Radiometer for Atmospheric Research," *Radio Science*, **36**, 2001, pp. 621-638.

36. F. T. Ulaby, R. K. Moore, and A. K. Fung, *Microwave Remote Sensing, Active and Passive. Volume 1, Microwave Remote Sensing Fundamentals and Radiometry*, Reading, Massachusetts, Addison-Wesley Publishing Company, 1981.

37. N. Skou, *Microwave Radiometer Systems: Design and Analysis*, Norwood, Massachusetts, Artech House, Inc., 1989.

38. L. Martin, A. Lüdi and C. Mätzler, "Tropospheric Monitoring with ASMUWARA," Proc. 6th International Symposium on Tropospheric Profiling (ISTP): Needs and Technologies, Leipzig, Germany, September 14-20, 2003 (also available from http://istp2003.tropos.de:8085/).

39. M. D. Jacobson and W. M. Nunnelee, "Design and Performance of a Spinning Flat Reflector for Millimeter-Wave Radiometry," *IEEE Transactions on Geoscience and Remote Sensing*, **35**, 1997, pp. 464-466.

40. M. J. Brittcliffe and R. C. Clauss, "The Effects of Water on the Noise-Temperature Contribution of Deep Space Network Microwave Feed Components," TMO Progress Report 42-145, May 15, 2001; http://tmo.jpl.nasa.gov/tmo/progress_report/42-145/145G.pdf.

41. S. Crewell, C. Simmer, A. Feijt and E. van Meijgaard, "CLIWA-NET Baltex Cloud Liquid Water Network," final report, BALTEX Report No. 26, ISSN 1681-6471.

42. J. Hach, "A Very Sensitive Airborne Radiometer Using Two Reference Temperatures," *IEEE Transactions on Microwave Theory and Techniques*, **MTT-16**, 9, 1968, pp. 629-636.

43. A. B. Tanner, A. L. Riley, "Design and Performance of a High-Stability Water Vapor Radiometer," *Radio Science*, **38**, 3, 2003, 8050, doi:10.1029/2002RS002673.

44. Y. Han and E. R. Westwater, "Analysis and Improvement of Tipping Calibration for Ground-Based Microwave Radiometers," *IEEE Transactions on Geoscience and Remote Sensing*, **GRS-38**, 2003, pp. 1260-1277.

45. E. R. Westwater, "Ground-based Microwave Remote Sensing of Meteorological Variables," in Michael A. Janssen (ed.), *Atmospheric Remote Sensing by Microwave Radiometry*, New York, J. Wiley & Sons, Inc., 1993, pp. 145-213.

46. R. Peter and N. Kämpfer, "Radiometric Determination of Water Vapor and Liquid Water and its Validation with other Techniques," *Radio Science,* **97**, D16, 1992, pp. 18173-18183.

47. C. Mätzler. "Ground-Based Observations of Atmospheric Radiation at 5, 10, 21, 35 and 94 GHz," *Radio Science*, **27**, 1992, pp. 403-415.

48. T. Ingold, R. Peter, and N. Kämpfer, "Weighted Mean Tropospheric Temperature and Transmittance Determination at Millimeter-Wave Frequencies for Ground-Based Applications," *Radio Science*, **33**, 1998, pp. 905-918.

49. R. Peter and B. Schmid, "Comparison of Columnar Water Vapor Determined from Microwave Emission and Solar Transmission Measurements," CWV4 in Proceedings Of the *Topical Symposium on Combined Optical-Microwave Earth and Atmosphere Sensing*, Albuquerque, NM, March 1993, pp. 193-198 (IEEE Cat. 93TH0519-9).

50. T. Ingold, B. Schmid, C. Mätzler, P. Demoulin, and N. Kämpfer, "Modeled and Empirical Approaches for Retrieving Columnar Water Vapor from Solar Transmittance Measurements in the 0.72, 0.82 and 0.94 μm Absorption Bands," *Journal of Geophysical Research*, **105**, D19, 2000, pp. 24327-24343.

51. C. Mätzler, L. Martin, G. Guerova, and T. Ingold, "Assessment of Integrated-Water-Vapour Data at Bern from GPS, Sun Photometry, Microwave Radiometry and Radiosonde," Proc. 2nd Workshop of COST Action 716, Exploitation of Ground-based GPS for Meteorology, GFZ Potsdam, January 28-29, 2002.

52. J. Wang, P. Racette, and L. A. Chang, "MIR Measurements of Atmospheric Water Vapor Profiles," *IEEE Transactions on Geoscience and Remote Sensing*, **GRS-35**, 1997, pp. 212-223.

53. J. Morland "TROWARA – Tropospheric Water Vapour Radiometer, Radiometer Review and New Calibration Model," IAP Research Report No. 2002-15, 2002.

54. D. Cimini, J. A. Shaw, Y. Han, E. R. Westwater, V. Irisov, V. Leuski, and J. H. Churnside, "Air Temperature Profile and Air-Sea Temperature Difference Measurements by Infrared and Microwave Scanning Radiometers," *Radio Science*, **38**, 3, 8045, 2003, doi:10.1029/2002RS002632.

55. F. Solheim, J. Godwin, E. Westwater, Y. Han, S. Keihm, K. Marsh, R. Ware, "Radiometric Profiling of Temperature, Water Vapor, and Liquid Water Using Various Inversion Methods," *Radio Science*, **33**, 1998, pp. 393-404.

56. C. Mätzler, "Messung der Wärmestrahlung der Erdoberfläche im Mikrowellengebiet," Diplomarbeit, IAP University of Bern, April 1970 (in German).

57. S. Twomey, *Introduction to the Mathematics of Inversion in Remote Sensing and Indirect Measurements*, New York, Elsevier, 1977.

58. A. N. Tikhonov and V. Y. Arsenin, *Solutions of Ill-Posed Problems*, Washington, DC, V.H. Winston and Sons, 1977.

59. J. H. Churnside, T. A. Stermitz, and J. A. Schroeder, "Temperature Profiling with Neural Network Inversion of Microwave Radiometer Data," *Journal of Atmospheric and Oceanic Technology*, **11**, 1994, pp. 105-109.

60. F. Del Frate and G. Schiavon, "A Combined Natural Orthogonal Functions/Neural Network Technique for Radiometric Estimation of Atmospheric Profiles," *Radio Science*, **33**, 1998, pp. 405-410.

61. W. M. Ledskam and D. H. Staelin, "An Extended Kalman-Bucy Filter for Atmospheric Temperature Profile Retrieval with a Passive Microwave Sounder," *Journal of Applied Meteorology*, **17**, 1978, pp. 1023-1033.

62. H. E. Moteller, L. L. Strow, and L. McMillin, and J. A. Gualtieri, "Comparison of Neural Networks and Regression-Based Methods for Temperature Retrievals," *Applied Optics*, **34**, 1995, pp. 5390-5397.

63. J. Askne and E. R. Westwater, "A Review of Ground-Based Remote Sensing of Temperature and Moisture by Passive Microwave Radiometers," *IEEE Transactions on Geoscience and Remote Sensing*, **GRS-24**, 1986, pp. 340-352.

64. N. A. Phillips, L. M. McMillin, D. Wark, and A. Gruber, "An Evaluation of Early Operational Temperature Soundings from TIROS-N," *Bulletin of the American Meteorological Society*, **60**, 1979, pp. 1188-1197.

65. A. Gelb, *Applied Optimal Estimation*, Cambridge, Massachusetts, MIT Press, 1988.

66.R. G. Brown and P. Y. C. Hwang, *Introduction to Random Signals and Applied Kalman Filtering*, New York, J. Wiley & Sons, 1997.

67.J. C. Derber and W.-S. Wu, "The Use Of TOVS Cloud-Cleared Radiances in the NCEP SSI Analysis System," *Monthly Weather Review*, **126**, 1998, pp. 2287-2302.

68. G. Ohring, K. Michell, M. Ji, S. Lord, and J. Derber, "Applications of Satellite Remote Sensing in Numerical Weather and Climate Prediction," *Advances in Space Research*, **30**, 2002, pp. 2433-2439.

69.U. Löhnert, U. S. Crewell, A. Macke, and C. Simmer, "Profiling Cloud Liquid Water by Combining Active and Passive Microwave Measurements with Cloud Model Statistics," *Journal of Atmospheric and Oceanic Technology*, **18**, 2001, pp. 1354-1366.

70.A. S. Frisch, G. Feingold, C. W. Fairall, T. Uttal, and J. B. Snider, "On Cloud Radar and Microwave Measurements of Stratus Cloud Liquid Water Profiles," *Journal of Geophysical Research*, **103**, 1998, pp. 23195-23197.

71.S. Crewell and U. Löhnert, "Accuracy of Cloud Liquid Water Path from Ground-Based Microwave Radiometry. Part II. Sensor Accuracy and Synergy," *Radio Science*, **38**, 3, 2003, doi:10.1029/2002RS002634.

72.E. R. Westwater, "Ground-Based Passive Probing Using the Microwave Spectrum of Oxygen," *Radio Science Journal of Research of the NBS* 9D, 9, 1965, pp. 1201-1211.

73. K. P. Gaikovich., E. N. Kadygrov, A. S Kosov, A. V. Troitskiy, "Thermal Sounding of the Boundary Layer of the Atmosphere at the Center of the Line of Oxygen Absorption," *Izvestia vuzov, Radiophysica*, **35**, 2, 1992, pp. 130-136.

74.J. Güldner and D. Spänkuch, "Remote Sensing of the Thermodynamic State of the Atmospheric Boundary Layer by Ground-Based Microwave Radiometry," *Journal of Atmospheric and Oceanic Technology*, **18**, 2001, pp. 925-933.

75.J. E. Liljegren, E. Clothiaux, S. Kato, and B. Lesht, "Initial Evaluation of Profiles of Temperature, Water Vapor and Cloud Liquid Water from a New Microwave Profiling Radiometer," *Proceedings of the 5th Symposium on Integrated Observing Systems*, Albuquerque, NM, American Meteorological Society, 2001

76.T. Nehrkorn and C. Grassotti, "Mesoscale Variational Assimilation of Profiling Radiometer Data," 16th Conference on Numerical Weather Prediction, Seattle, WA, American Meteorological Society, 2004.

77.A. Lüdi, L. Martin, and C. Mätzler, "The Retrieval of Temperature Profiles with the Ground-Based Radiometer System ASMUWARA," IAP Research Report No. 2003-13, September 2003.

78.L. Martin, "Microwave Transmission and Emission Measurements for Tropospheric Monitoring," Inauguraldissertation, Phil.-nat. Fakultät, Universität Bern, Juni 2003.

79.A. Siegenthaler, O. Lezeaux, D. G. Feist, and N. Kämpfer, "First Water Vapor Measurements at 183 GHz from the High Alpine Station Jungfraujoch," *IEEE Transactions on Geoscience and Remote Sensing*, **GRS-39**, 2001, pp. 2084-2086.

80.E. R. Westwater, J. B. Snider, and A. C. Carlson, "Experimental Determination of Temperature Profiles by Ground-Based Microwave Radiometry," *Journal of Applied Meteorology*, **14**, 4, 1975, pp. 524-539.

81.E. R. Westwater, Y. Han, V. G. Irisov, V. Leuskiy, E. N. Kadygrov, and S. A. Viazankin, "Remote Sensing of Boundary-Layer Temperature Profiles by a Scanning 5-Mm Microwave Radiometer and RASS: A Comparison Experiment," *Journal of Atmospheric and Oceanic Technology*, **16**,7, 1999, pp. 805-818.

82.U. Löhnert, S. Crewell, and C. Simmer, "An Integrated Approach towards Retrieving Physically Consistent Profiles of Temperature, Humidity and Cloud Liquid Water," *Journal of Applied Meteorology*, 2004 (in press).

83.B. B. Stankov, E. R. Westwater, and E. E. Gossard, "Use of Wind Profiler Estimates of Significant Moisture Gradients to Improve Humidity Profile Retrieval," *Journal of Atmospheric and Oceanic Technology*, **13**, 6, 1996, pp. 1285-1290.

84.G. M. Stokes and S. E. Schwartz, "The Atmospheric Radiation Measurement (ARM) Program: Programmatic Background and Design of the Cloud and Radiation Testbed," *Bulletin of the American Meteorological Society*, **75**, 1994, pp. 1201-1221.

85.T. P. Ackerman and G. M. Stokes, "The Atmospheric Radiation Measurement Program," *Physics Today*, **56**, 1, 2003, pp. 38-44.

86.P. Zuidema, B. Baker, Y. Han, J. Intrieri, J. Key, P. Lawson, S. Matrosov, M. Shupe, R. Stone, and T. Uttal, "An Arctic Springtime Mixed-Phase Cloudy Boundary Layer observed during SHEBA," submitted to *Journal of Atmospheric Sciences*, 2004.

87.M. D. Shupe, T. Uttal, S. Matrosov, and A. S. Frisch, "Cloud Water Contents and Hydrometeor Sizes during the FIRE Arctic Cloud Experiment," *Journal of Geophysical Research*, **106**, D14, 2001, pp. 15015-15028.

88.B. B. Stankov, B. E. Martner, and M. K. Politovich, "Moisture Profiling of the Cloudy Winter Atmosphere Using Combined Remote Sensors," *Journal of Atmospheric and Oceanic Technology*, **12**, 1995, pp. 488-510.

89.V. D. Stepanenko, G. G. Schukin, L. P. Bobylev, and S. Yu. Matrosov, *Radioteplolocatziya v Meteorologiya* (*Microwave Radiometry in Meteorology*), Leningrad, Gidrometeozdat, 1987 (in Russian).

90.J. C. Liljegren, "Improved Retrievals of Temperature and Water Vapor Profiles with a Twelve-Channel Radiometer," *2004 Proc. of the Eighth Symposium on IOAS-AOLS*, American Meteorological Society, January 11-15, 2004, Seattle, WA.

91.E. R. Westwater, P. E. Racette, and D. Cimini, "The Arctic Winter Millimeter-Wave Radiometric Experiment: Summary, Conclusions, and Recommendations," *Proc. of 11th Atmospheric Radiation Measurement (ARM) Science Team Meeting*, March 19-23, 2001 (available at http://www.arm.gov/docs/documents/technical/conf_0103/index.html).

92.E. R. Westwater, M. Klein, and V. Leuski, A. Gasiewsk, T. Uttal, D. Hazen, D. Cimini, V. Mattioli, B. L. Weber, S. Dowlatshahi,J. A. Shaw, J. Liljegren, B. M. Lesht, and B. D. Zak, "The 2004 North Slope of Alaska Arctic Winter Radiometric Experiment," *Proc. of 14th Atmospheric Radiation Measurement (ARM) Science Team Meeting*, Albuquerque, New Mexico, March 22-26, 2004 (available at http://www.arm.gov/docs/documents/technical/conf_0304/index.html).

93.Y. Han and E. R. Westwater, "Remote Sensing of Tropospheric Water Vapor and Cloud Liquid Water by Integrated Ground-Based Sensors," *Journal of Atmospheric and Oceanic Technology*, **12**, 5, 1995, pp. 1050-1059.